



Deposited via The University of Leeds.

White Rose Research Online URL for this paper:

<https://eprints.whiterose.ac.uk/id/eprint/101494/>

Version: Accepted Version

Article:

Schiffrin, B, Calabrese, AN, Devine, PWA et al. (2016) Skp is a multivalent chaperone of outer membrane proteins. *Nature Structural and Molecular Biology*, 23 (9). pp. 786-793. ISSN: 1545-9993

<https://doi.org/10.1038/nsmb.3266>

(c) 2016, Nature American, Inc. This is an author produced version of a paper published in *Nature Structural & Molecular Biology*. Uploaded in accordance with the publisher's self-archiving policy.

Reuse

Items deposited in White Rose Research Online are protected by copyright, with all rights reserved unless indicated otherwise. They may be downloaded and/or printed for private study, or other acts as permitted by national copyright laws. The publisher or other rights holders may allow further reproduction and re-use of the full text version. This is indicated by the licence information on the White Rose Research Online record for the item.

Takedown

If you consider content in White Rose Research Online to be in breach of UK law, please notify us by emailing eprints@whiterose.ac.uk including the URL of the record and the reason for the withdrawal request.

1 Skp is a multivalent chaperone of outer membrane proteins

2

3 **Bob Schiffrin^{1,2,4}, Antonio N. Calabrese^{1,2,4}, Paul W. A. Devine^{1,2}, Sarah A. Harris^{1,3},**

4 **Alison E. Ashcroft^{1,2}, David J. Brockwell^{1,2}, Sheena E. Radford^{1,2}**

5

6 ¹Astbury Centre for Structural Molecular Biology, ²School of Molecular and Cellular Biology,

7 University of Leeds, Leeds, UK, ³School of Physics and Astronomy, University of Leeds,

8 Leeds, UK. ⁴These authors contributed equally to this work. Correspondence should be

9 addressed to S.E.R. (s.e.radford@leeds.ac.uk), D.J.B. (d.j.brockwell@leeds.ac.uk) or A.E.A.

10 (a.e.ashcroft@leeds.ac.uk).

11

12

13 **Abstract**

14 The trimeric chaperone Skp sequesters outer membrane proteins (OMPs) within a

15 hydrophobic cage, preventing their aggregation during transport across the periplasm in

16 Gram negative bacteria. Here, we study the interaction between *Escherichia coli* Skp and

17 five OMPs of varying size. Investigations of the kinetics of OMP folding reveal that greater

18 Skp:OMP ratios are required to prevent the folding of 16-stranded OMPs compared with

19 their 8-stranded counterparts. Ion mobility spectrometry-mass spectrometry (IMS-MS) data,

20 computer modelling and molecular dynamics simulations provide evidence that 10- to 16-

21 stranded OMPs are encapsulated within an expanded Skp substrate cage. For OMPs which

22 cannot be fully accommodated in the expanded cavity, sequestration is achieved by binding

23 of an additional Skp trimer. The results suggest a new mechanism for Skp chaperone activity

24 involving coordination of multiple copies of Skp to protect a single substrate from

25 aggregation.

26 β -barrel outer membrane proteins (OMPs) perform numerous essential and diverse
27 functions in the outer membrane (OM) of Gram negative bacteria. After synthesis in the
28 cytoplasm, OMPs are translocated across the inner membrane, and then must traverse the
29 periplasm before reaching the OM, where the β -barrel Assembly Machinery (BAM) complex
30 folds and inserts them¹⁻⁵. While the periplasmic chaperones Skp and SurA are considered
31 the major OMP chaperones in *E. coli*, a network of folding factors is involved in OMP
32 assembly, including Trigger Factor and SecB in the cytoplasm, and FkpA and DegP in the
33 periplasm^{1,6,7}. Periplasmic chaperones act without an external energy source (unlike many of
34 the Hsp chaperones⁸), as the periplasm is devoid of ATP⁵, and bind and release their
35 substrates by mechanisms that are not well understood⁷.

36

37 The holdase chaperone Skp protects OMPs against misfolding and aggregation during their
38 transit between the inner and outer membranes⁹⁻¹¹. Skp has broad substrate specificity¹²,
39 with reported affinities for its substrates in the low nanomolar range^{13,14}. Skp is a functional
40 homotrimer (referred to herein as Skp) with a 'jellyfish'-like architecture (**Fig. 1a**)^{10,11},
41 consisting of three α -helical 'legs' that extend 60 Å away from the 'body' domain; a 9-
42 stranded β -barrel which mediates trimerisation^{10,11}. The three subunits of Skp form a
43 hydrophobic cavity inside which OMP clients are bound^{9,12,15,16}, with previous studies
44 suggesting a 1:1 stoichiometry for all Skp:OMP complexes^{13,17,18}. These 1:1 stoichiometries
45 have been proposed using tryptophan fluorescence (Skp complexes formed with tOmpA (19
46 kDa)¹³, NalP (32 kDa)¹³, OmpG (33 kDa)¹³, OmpA (35 kDa)^{13,17} and BamA (89 kDa)¹³), by
47 NMR (OmpX (16 kDa) and tOmpA (19 kDa)¹⁵) and by fluorescence correlation spectroscopy
48 (OmpC (38 kDa)¹⁸). The Skp hydrophobic cavity has been estimated to be able to
49 accommodate folded proteins of ~25 kDa¹⁰, but many OMPs known to interact with Skp are
50 considerably larger (e.g. the 22-stranded BtuB and the 26-stranded LptD are 66 kDa and 87

51 kDa, respectively)¹². This raises fundamental questions about the structural alterations that
52 must occur for Skp to accommodate its larger substrates.

53

54 To investigate the mechanism by which Skp sequesters OMPs of different sizes, we used
55 kinetic studies of OMP folding complemented with electrospray ionization-ion mobility
56 spectrometry-mass spectrometry (ESI-IMS-MS) analyses to examine the interactions of Skp
57 with five diverse OMPs: 1) tOmpA, the 8-stranded transmembrane domain of OmpA¹⁹; 2)
58 PagP, an 8-stranded acyl transferase enzyme²⁰; 3) OmpT, a 10-stranded protease²¹; 4)
59 OmpF, a 16-stranded trimeric porin²²; and 5) tBamA, the 16-stranded transmembrane
60 domain of the BamA OMP insertase²³ (**Fig. 1b-f, Supplementary Table 1**). We find that the
61 concentration of Skp required to prevent OMP insertion into *di*_{C11:0}PC liposomes increases
62 as the mass of client OMP increases, suggesting that the sequestration mechanism of Skp is
63 altered for larger OMP clients. ESI-IMS-MS and computer modelling were used to examine
64 the conformations of Skp:OMP complexes and provided evidence that the core of Skp
65 expands to accommodate the larger OMPs, with the largest clients requiring the formation of
66 2:1 Skp:OMP assemblies to completely sequester the polypeptide chain. Combined, the
67 results provide a new understanding of how Skp is able to bind, chaperone and release
68 substrates that vary dramatically in size, with expansion of the binding cage and/or formation
69 of multivalent complexes allowing the chaperone to adapt to the demands of its clients.

70

71

72 [The main text (currently ~4,600 words) is over our limit of 4,000 words for Articles.
73 The Results are especially long, > 3,000 words; please trim Results to ~2,400 words]
74 Results are now ~2,590 words

75 **Results**

76 **Different Skp:OMP ratios are required to inhibit OMP folding**

77 To assess the effects of Skp on the folding and membrane insertion of OMPs of varied size,
78 folding assays were performed by diluting unfolded protein stock solutions (in 8 M urea) 33-
79 fold into buffer containing ~100 nm diameter synthetic $di_{C11:0}PC$ liposomes. The increase in
80 tryptophan fluorescence associated with folding was then measured as a function of time.
81 Maintaining a low protein concentration (0.4 μM) and a high lipid:protein ratio (3200:1)
82 enables folding to be monitored in a low final concentration of urea (0.24 M) without
83 interference from aggregation. This approach enables real time measurements of folding
84 that are complementary to SDS-PAGE based studies which have been used to provide
85 information about the fraction of folded (SDS-resistant) protein present at a particular time²⁴⁻
86 ²⁶.

87
88 To verify that the OMPs selected for study are able to fold into $di_{C11:0}PC$ liposomes and/or
89 interact with Skp under the experimental conditions selected, fluorescence emission spectra
90 of each OMP were measured in 8 M or 0.24 M urea in the absence of liposomes (in the latter
91 case with and without a two-fold molar excess of Skp). These spectra were then compared
92 with those of membrane inserted (folded) OMP obtained at the end point of the folding
93 reaction (**Fig. 2a-d**). Spectra of tOmpA, PagP, OmpF and tBamA folded into liposomes show
94 a characteristic blue-shift in λ_{max} and increase in fluorescence intensity compared with
95 spectra of the unfolded proteins in 8 M urea, indicating that a substantial fraction of all four
96 OMPs fold successfully into the liposomes employed. In the presence of Skp, the spectra of
97 tOmpA, OmpF and tBamA show decreases in λ_{max} and/or intensity compared with spectra of

98 these OMPs in buffer alone, demonstrating that these unfolded OMPs interact with Skp. For
99 PagP no change in fluorescence is observed in the presence of Skp, although these proteins
100 do interact, as shown in previous work²⁷.

101

102 The effect of Skp on OMP folding kinetics was next investigated. In the absence of Skp, the
103 OMPs fold with either single or double exponential kinetics (**Fig. 2a-d**), allowing extraction of
104 the folding rate constants (k_1 and k_2) (**Fig. 2a-d, Supplementary Table 2**). To verify that the
105 transients obtained reflect membrane insertion and folding, assays were performed in the
106 absence of lipids (**Supplementary Fig. 1**). A folding transient is observed only for OmpT in
107 the absence of lipid (**Supplementary Fig. 1e**), presumably reflecting folding of the large
108 extracellular region of OmpT which contains three tryptophan residues (**Supplementary Fig.**
109 **1f**). For all other OMPs, no change in fluorescence was observed over time in the absence
110 of lipid, indicating the formation of a stable soluble form, as previously reported^{13,27}. The
111 folding kinetics of OMPs that had been pre-incubated with Skp at molar ratios ranging from
112 1:1 to 4:1 (chaperone:client) (where Skp concentrations are in trimer equivalents, see Online
113 Methods) were then measured by adding the pre-formed complexes to *diC*_{11:0}PC liposomes
114 and monitoring OMP folding by fluorescence spectroscopy (**Fig. 2a-d, Supplementary Fig.**
115 **2**). The results show that at a substrate concentration of 0.4 μ M, a 2-fold molar excess of
116 Skp is sufficient to prevent tOmpA and PagP folding into liposomes (**Fig. 2a, b,**
117 **Supplementary Fig. 2a, b**). We have previously shown that while incubation of Skp with
118 PagP at a 2:1 ratio prevents OMP folding over a 2 h timescale, overnight incubation with
119 liposomes allows OMP release and folding to equivalent yields as in the absence of Skp²⁷.
120 For both of the 8-stranded OMPs tOmpA and PagP, a 1:1 Skp:OMP ratio retards folding,
121 while a 2:1 ratio prevents folding over the timescale of the experiment. By contrast, pre-
122 incubation of OmpF and tBamA with a 2-fold excess of Skp decreases the folding rate, but
123 does not prevent folding (**Fig. 2c, d, Supplementary Fig. 2c, d**). However, pre-incubation

124 with a 4-fold excess of Skp inhibits folding of these larger proteins over the timescale of the
125 experiment (**Fig. 2c, d, Supplementary Fig. 2c, d**). The results suggest, therefore, that
126 complete sequestration of larger OMP barrels requires the binding of more than one copy of
127 Skp.

128

129 **Stoichiometries of Skp:OMP assemblies studied by ESI-MS**

130 To gain insights into the architectures of Skp:OMP assemblies, we exploited ESI-MS
131 coupled with IMS to analyze different Skp:OMP complexes within multicomponent mixtures.
132 Skp assemblies with tOmpA, PagP, OmpT, OmpF and tBamA were prepared, and mass
133 spectra acquired using instrumental conditions that allow non-covalent interactions to be
134 retained *in vacuo* (termed non-covalent or “native” MS)²⁸⁻³⁰ (see Online Methods) (**Fig. 3,**
135 **Supplementary Fig. 3a-f, Supplementary Table 3**). The results show that all five Skp:OMP
136 assemblies are sufficiently stable to survive the ESI process and be transferred into the gas
137 phase for analysis.

138

139 Several reports have suggested that Skp binds unfolded OMPs ranging from 16-89 kDa (8-
140 16 β -strands in the native state) with a 1:1 stoichiometry^{13,15,17,18}. By contrast, the mass
141 spectra shown in **Fig. 3** reveal that the stoichiometry of these assemblies is dependent on
142 the size of the OMP client, consistent with the kinetic traces described above. Thus, tOmpA
143 and PagP (8-stranded OMPs) bind only one Skp, whilst the larger OMPs, OmpT, OmpF and
144 tBamA (10- and 16-stranded OMPs) bind up to two copies of Skp. Peaks corresponding to
145 monomeric Skp subunits were also observed ($m/z \sim 2000$) (**Fig. 3**), indicating either that
146 some dissociation of the assembly is occurring in-source, and/or reflecting the population of
147 monomeric subunits in solution^{31,32}. Interestingly, a 2:1 assembly is the predominant
148 complex observed in the spectrum for the largest 16-stranded OMP studied, tBamA, despite

149 being formed by mixing Skp with tBamA at a 1:1 molar ratio (**Fig. 3f**). A 2:1 Skp:OMP
150 assembly was also observed for full-length BamA (**Supplementary Fig. 4a,b**). To confirm
151 that the Skp:OMP stoichiometry observed using ESI-MS reflects the stoichiometry in solution,
152 we performed chemical cross-linking with bis(sulfosuccinimidyl)suberate (BS3), followed by
153 SDS-PAGE analysis of Skp pre-incubated with full-length OmpA or full-length BamA. In the
154 cross-linked Skp:OmpA samples, a 1:1 assembly was observed (**Supplementary Fig. 5a-d**)
155 whereas in the Skp:BamA samples a band consistent with a complex with a 2:1
156 stoichiometry (but no 1:1 Skp:BamA complex) was observed (**Supplementary Fig. 5e-g**).

157

158 **Insights into Skp:OMP complex structure from ESI-IMS-MS**

159 How Skp binds its OMP clients of larger size was next analyzed using ESI-IMS-MS. IMS
160 measures the mobility of ions through an inert gas-filled chamber under the influence of a
161 weak electric field, with the drift time (mobility) of an ion in this environment dependent on its
162 mass, size and charge^{28,33}. Here, we used travelling wave IMS-MS^{28,33}, for which calibration
163 of the measured drift time data can be performed to obtain rotationally averaged collision
164 cross-sections (CCSs), to provide insight into the conformations of Skp and the Skp:OMP
165 assemblies. IMS data were acquired for all of the assemblies studied (**Fig. 4a-f**,
166 **Supplementary Fig. 3a-f**), and compared with known structures where available, or with
167 models of the Skp:OMP complexes for which there are no high resolution structural data.

168

169 **Fig. 4a-f** displays the CCS distributions of the observed ions originating from Skp and 1:1
170 Skp:OMP complexes, normalized to spectral intensity (a representative dataset is shown
171 from three independent experiments). The modal CCSs are also plotted as a function of
172 charge state in **Fig. 4g (Supplementary Table 4)**. Interestingly, the CCSs of the Skp ions
173 (**Fig. 4g**) are smaller than expected based on the published Skp crystal structure (the modal

174 CCS at the lowest observed charge state, which is least affected by Coulombic repulsion³⁴,
175 was 37.9 nm², approximately 25 % lower than the expected value of 45.7 nm² derived from
176 the crystal structure (**Fig. 4g**). Molecular dynamics simulations (**Supplementary Fig. 6**,
177 **Supplementary Data Sets 1 and 2**) revealed that the assembly collapses in the gas phase,
178 resulting in a structure with CCS of 37.3 ± 1.9 nm² (**Fig. 4g**).

179

180 Binding of Skp to the 8-stranded tOmpA and PagP (**Fig. 4g**) results in ions with increased
181 CCS compared with Skp alone. The CCSs of the ions observed (45.6 nm² and 45.8 nm² for
182 Skp:tOmpA and Skp:PagP, respectively, at the lowest observed charge state) compare
183 favorably with the CCS predicted from the crystal structure of Skp alone (45.7 nm²),
184 supporting the notion that these assemblies are specific complexes in which the OMP is
185 located within the central Skp cavity, preventing collapse of the chaperone in the gas
186 phase^{15,16}. Consistent with this, the Skp:OMP complexes sample a narrower conformational
187 ensemble compared with Skp alone, measured by the width at half height of the mobility
188 peaks observed (**Fig. 4a-c**). Complexation with tOmpA and PagP thus packs the
189 hydrophobic cavity of Skp resulting in a narrower conformational ensemble, consistent with
190 previous data¹⁵.

191

192 Interestingly, the 1:1 Skp:OMP assemblies of the larger OMPs studied (OmpT, OmpF and
193 tBamA) (**Fig. 4g**) have increased CCSs (51.4-54.2 nm²) compared with the Skp:tOmpA and
194 Skp:PagP assemblies (~46 nm²). These data, together with mismatch between the volume
195 of Skp's cavity and the volume likely to be occupied by larger OMP clients in the 'fluid
196 globule' state¹⁵, suggest that the central cavity expands in size to encapsulate these species,
197 consistent with recent SANS data³⁵. However, the kinetic data (**Fig. 2c,d**) indicate that Skp
198 expansion is insufficient to fully sequester these larger OMPs in a 1:1 complex.

199

200 Plotting the increase in CCS as a function of molecular weight for Skp and all complexes
201 (**Fig. 4h**), including 2:1 Skp:OMP assemblies (**Supplementary Fig. 3g**), reveals that the
202 data fit to a globular model, irrespective of client size. The complexes exhibit an effective gas
203 phase density of $0.33 \text{ Da}\cdot\text{\AA}^{-3}$, similar to values reported for other protein complexes³³, and
204 consistent with recent calculations of the CCSs of globular proteins in the PDB³⁶.

205

206 **Modelling of larger OMPs in complex with two copies of Skp**

207 Models for the architecture of Skp in complex with OmpT, tBamA or OmpF were next
208 generated to determine how Skp and a partially folded OMP may interact. Four different
209 models were constructed. As a starting point, encapsulated tOmpA was modelled as a
210 sphere with a radius of 20 Å (**Fig. 5a**) which has a volume of $33,500 \text{ \AA}^3$, consistent with
211 previous estimates^{10,15}. We assumed that the amino acid density for non-native OMPs bound
212 to Skp is independent of the mass of the OMP studied, consistent with the MS data
213 presented above. Therefore, to model a 16-stranded OMP, we assumed a spherical volume
214 of $\sim 67,000 \text{ \AA}^3$ giving a radius of $\sim 25 \text{ \AA}$, and generated a Skp model with its three subunits
215 surrounding a sphere of this size (**Fig. 5b**). The theoretical CCS of the resulting structure
216 (50.4 nm^2) (**Fig. 4g**) is in good agreement with the measured CCS values for 1:1 Skp:OmpT,
217 Skp:OmpF and Skp:tBamA complexes (51.4 , 51.8 and 54.2 nm^2 , respectively) (**Fig. 4g**,
218 **Supplementary Table 4**). The results suggest, therefore, that 1:1 Skp:OMP complexes with
219 larger OMPs, involve an expanded Skp cavity.

220

221 Next, we generated models of the 2:1 Skp:OMP complexes, theorizing that Skp could
222 arrange in a side-by-side configuration, in either a parallel or antiparallel arrangement (**Fig.**
223 **5c,d**), with the OMP represented by a capsule. The theoretical CCSs of these assemblies

224 were determined to be 79.1 and 78.2 nm², respectively (**Fig. 4g**). Alternatively, we
225 considered a model in which the OMP substrate (represented by a sphere with a radius of
226 ~25 Å) may be encapsulated by two interlocked copies of Skp (**Fig. 5e**), which results in a
227 complex with a theoretical CCS of 73.5 nm² (**Fig. 4g**). All three values are in good
228 agreement with the measured CCS values for 2:1 Skp:OmpT, Skp:OmpF and Skp:tBamA
229 complexes (71.7, 71.2 and 72.8 nm², respectively) (**Fig. 4g, Supplementary Table 4**).

230

231 **Molecular dynamics simulations to model Skp:OMP complexes**

232 To model the Skp:OMP complexes further and aid their visualization, we performed a series
233 of molecular dynamics simulations. A simulation of apo-Skp in explicit solvent over 100 ns
234 demonstrated that the individual subunits are highly dynamic and flexible. Each subunit
235 undergoes a transition to an 'open' state, in which subunit helices splay from the central axis,
236 resulting in an expanded central cavity, consistent with previous MD studies^{18,35}
237 (**Supplementary Fig. 7a-c, Supplementary Data Sets 1 and 3, Supplementary Video 1**).

238 The average radius of gyration (R_g) of Skp from the simulation (31.5 Å) is in good agreement
239 with published SANS data (~33 Å)³⁵. This R_g is ~10 % higher than that predicted from the
240 crystal structure, indicating that dynamic motions of the Skp subunits observed in the
241 simulation likely reflect those in solution. In the two Skp crystal structures solved to date^{10,11},
242 the lower section of one of the subunits is unresolved, indicating flexibility, and the angles
243 with which the Skp subunits extend away from the 'body' domain are different for each of the
244 subunits in the two structures^{10,11}. The subunits in the crystal structure of the
245 heterohexameric eukaryotic chaperone prefoldin (**Fig. 5f**) also make different angles with
246 respect to the multimerisation domain, which has also been suggested to indicate
247 conformational flexibility that may be functionally relevant³⁷.

248

249 Next, we generated models of tOmpA (8-stranded) and tBamA (16-stranded) alone in an
250 unfolded, extended conformation, and simulated their behavior in solvent (mimicking the
251 situation in which OMPs are diluted from 8 M urea). In each case, the OMPs collapse rapidly
252 to an approximately globular form (**Supplementary Fig. 7d,e, Supplementary Video 2**). A
253 model of the 1:1 Skp:tOmpA complex was then generated by placing the collapsed tOmpA
254 structure within the cavity of Skp in an ‘open’ conformation from the simulation of apo-Skp
255 (**Supplementary Fig. 7b**) and relaxing the resulting structure *in vacuo*. In the simulation, the
256 subunits of Skp collapse rapidly around the tOmpA substrate resulting in a structure with a
257 CCS value ($43.7 \pm 1.2 \text{ nm}^2$) in excellent agreement with that measured by ESI-IMS-MS (45.6
258 $\pm 0.1 \text{ nm}^2$), suggesting that, at least in the gas phase, Skp “clamps” around the substrate
259 (**Fig. 6a,b, Supplementary Video 3**). A model for the gas-phase 2:1 Skp:tBamA complex
260 was created by placing the collapsed tBamA structure in the hydrophobic cavity formed by
261 two copies of Skp in their ‘open’ conformations. A side-by-side parallel orientation (**Fig. 6c**)
262 was chosen based on the striking resemblance of this model to the structure the eukaryotic
263 prefoldin chaperone³⁷ (**Fig. 5f**). The size of the collapsed tBamA model clearly exceeds the
264 maximal dimensions of the cavity of a single Skp observed in an ‘open’ conformation (**Fig.**
265 **6c**). Simulation of the 2:1 Skp:tBamA complex *in vacuo* showed that the Skp subunits also
266 rapidly “clamp” around the tBamA substrate creating a complex with a CCS value (74.4 ± 1.4
267 nm^2) again in good agreement with the IMS data ($72.8 \pm 0.2 \text{ nm}^2$) (**Fig. 6d, Supplementary**
268 **Video 4**). Thus, the CCS data obtained from both experiment and simulation
269 (**Supplementary Table 5**) are consistent with a model in which multivalent Skp binding is
270 necessary to sequester OMPs that exceed the dimensions of the Skp cavity.

271

272 To provide evidence that a similar “clamping” motion of Skp around its OMP substrates
273 could occur in solution, we performed analogous MD simulations of Skp:tOmpA and 2:1
274 Skp:tBamA complexes in explicit solvent. In these simulations Skp subunits are also

275 observed wrapping around their OMP substrates (**Fig. 7a,b, Supplementary Videos 5,6**),
276 with 'clamping' movements similar to those observed in the gas-phase simulations (**Fig. 6**).
277 The complexes formed are stable over 100 ns (**Fig. 7c,d**) and have larger calculated CCS
278 values ($56.5 \pm 0.3 \text{ nm}^2$ and $101.2 \pm 6.0 \text{ nm}^2$ for Skp:tOmpA and 2:1 Skp:tBamA, respectively)
279 than those following gas-phase simulation ($43.7 \pm 1.2 \text{ nm}^2$ and $74.4 \pm 1.4 \text{ nm}^2$ for Skp-
280 tOmpA and 2:1 Skp-tBamA, respectively). These data are consistent with a model in which
281 the subunits of Skp are dynamic, resulting in expansion of the hydrophobic cavity that allows
282 entry of substrates of varying sizes, prior to the Skp subunits 'wrapping' around the
283 sequestered client to protect it from aggregation until folding into the bilayer can take place.

284

285 **Discussion**

286 Major advances in the understanding of the cascade of molecular chaperones and folding
287 catalysts involved in OMP biogenesis have been made in recent years, yet the molecular
288 details of how OMPs are bound by molecular chaperones, transported across the periplasm
289 and assembled into the outer membrane, without using the energy of ATP binding/hydrolysis,
290 remain unclear^{1,7,23}. Here, we have provided new insights into how Skp is able to chaperone
291 its broad array of OMP clients, including substrates which are too large to be accommodated
292 within its hydrophobic cavity. We have shown that Skp utilizes subunit dynamics to expand
293 the size of its client binding cavity and have demonstrated that Skp can function as a
294 multivalent chaperone in order to sequester and prevent aggregation of its larger OMP
295 clients. Further, we have used ESI-IMS-MS to gain structural insight into the 1:1 and 2:1
296 Skp:OMP complexes we have identified. Using kinetic refolding and ESI-IMS-MS data,
297 combined with MD simulations, we present models consistent with the experimental results
298 in which Skp sequesters larger OMPs by binding in a multivalent arrangement (side-by-side
299 parallel or anti-parallel, and/or via an interlocking structure) (**Fig. 5c-e**). The parallel side-by-
300 side model (**Fig. 5c**) bears a striking resemblance to the structure of the non-homologous
301 chaperone prefoldin (**Fig. 5f**)³⁷. The precise orientation(s) of Skp molecules in these
302 multivalent complexes will require more information to resolve, for example using cross-
303 linking experiments followed by MS/MS. Nonetheless, the biochemical, MS and MD results
304 presented indicate that the ability of Skp to chaperone OMPs ranging from 35-43 kDa in size
305 requires both subunit dynamics and its ability to function as a multivalent chaperone.

306

307

308

309 Skp has been shown *in vivo* to interact with much larger substrates than those investigated
310 here (19-43 kDa), including BtuB (66 kDa), FhuA (79 kDa) and LptD (87 kDa) which form β -
311 barrels composed of 22, 22, and 26 β -strands, respectively^{12,38}. It is likely these proteins also
312 form multivalent complexes with Skp and indeed recent data on the interaction between Skp
313 and FhuA is consistent with a greater than 1:1 Skp:OMP stoichiometry³⁹.

314

315 The results presented have implications for our understanding of how OMPs are chaperoned
316 by Skp in the periplasm, including the mechanisms of substrate binding and release. Our
317 atomistic MD trajectories of apo-Skp show that it exists in a wide range of open
318 conformations with large differences in the area of the cavity entrance formed between the
319 tips of its three subunits. Such conformational flexibility has been implicated in the
320 mechanisms of other ATP-independent chaperones^{40,41}. We propose that in rescuing
321 aggregation-prone proteins⁶ Skp could be thought of as analogous to a pair of 'calipers',
322 sampling open conformations prior to capture of its client, allowing it to adjust the volume of
323 its central cavity. In this model once the substrate has entered the Skp cavity, the Skp
324 subunits 'clamp down' to protect the exposed hydrophobic surfaces of the protein, in a
325 mechanism similar to those of other chaperones such as Trigger Factor or Hsp90⁴². For
326 substrates which are too large to be accommodated within the Skp substrate cavity,
327 additional copies of Skp recognize and engulf sections of the substrate not already
328 encapsulated. *In vivo* cross-linking evidence suggests that Skp can interact with OMPs as
329 they emerge from the SecYEG translocon⁴³. Thus it is possible that during translocation of
330 larger OMPs, the substrate is fed directly into the cavity of Skp and the chaperone's
331 maximum binding capacity would then be reached before the complete polypeptide chain is
332 translocated. Subsequent polypeptide chain emerging from the translocon could then be
333 bound by a second or more Skp(s), ensuring sequestration of the entire polypeptide
334 sequence so that periplasmic aggregation is prevented.

335

336 Recent equilibrium sedimentation experiments of Skp in the absence of substrate have
337 demonstrated a dynamic equilibrium between folded subunit monomers and trimers at
338 physiological concentrations³². Therefore, a possible alternative *in vivo* pathway to Skp-OMP
339 complex formation may involve sequential binding of monomer subunits to OMP substrates,
340 with Skp trimerization linked to (and indeed driven by) substrate binding. Sandlin *et al.* raise
341 the possibility that more diverse species of Skp could form around an unfolded OMP³².
342 However, for the complexes studied here only Skp-OMP complexes containing monomeric
343 Skp subunits in multiples of three are observed (**Fig. 3**), suggesting either that the trimeric
344 unit is the OMP binding species, or that complexes of other composition are unstable in the
345 gas-phase.

346

347 It has been proposed that transient exposure of the C-terminal OMP targeting sequence (β -
348 signal)^{44,45}, and its recognition by the BAM complex⁴⁶, triggers substrate release from Skp¹⁵.
349 The space between Skp subunits (~ 25 Å in the crystal structure¹⁰) and/or the inherent
350 dynamics of the complex may facilitate the transient solvent-exposure of regions of the OMP
351 substrate, permitting β -signal recognition. Consistent with this, the presence of BamA in
352 liposomes relieves the folding inhibition of OmpA by Skp *in vitro*⁴⁷. It is interesting to note
353 that in all 2:1 Skp:OMP models proposed here there remains a substantial distance (> 20 Å)
354 between the Skp subunits which would permit exposure of sections of the substrate
355 polypeptide required for BAM signalling and/or membrane insertion. The release of the OMP
356 from Skp is likely to be driven by the increased thermodynamic stability of the folded OMP
357 relative to the chaperone-bound state⁴⁸, and for OMPs that are bound to more than one Skp,
358 it is possible that individual copies of Skp are released sequentially in a process driven by
359 the free energy of OMP folding.

360

361 Chaperones utilize two general strategies to protect substrates from misfolding and
362 aggregation. In the first, substrates are chaperoned by sequential binding and release of
363 exposed hydrophobic surfaces along an extended polypeptide chain. This 'beads on a string'
364 model is typified by chaperones such as the Hsp70s and Trigger Factor^{8,49}. Alternatively,
365 aberrant interactions may be prevented by sequestration of the substrate from the cellular
366 environment within an enclosed space, as is the case for the 'cage-like' chaperonins such as
367 GroEL/ES and TriC^{8,49}. The data presented here suggest that Skp operates with a 'hybrid'
368 mechanism, employing both of these strategies to bind and encapsulate its OMP clients,
369 thereby preventing their aggregation and facilitating their delivery to the OM wherein folding
370 can successfully occur.

371

372 **Acknowledgements**

373 The plasmids containing the mature sequences of tOmpA, PagP, OmpA and BamA were
374 kindly provided by K. Fleming (John Hopkins University, USA)²⁵. Plasmid pET21b
375 (Novagen) containing the Skp gene was a gift from J. Bardwell (University of Michigan,
376 USA). We also thank S. Hiller (University of Basel, Switzerland) for kindly providing the
377 His-tagged Skp construct¹⁵, and S. Buchanan (NIH, USA) for the gift of plasmid BamAB-
378 pETDUET-1. We thank T. Watkinson (University of Leeds, UK) for expression and
379 purification of OmpT, and M. Jackson (University of Leeds, UK) for help with western blots,
380 and are also grateful for the assistance and advice of L. M. McMorran (University of Leeds,
381 UK) in the early stages of this work. This work was supported by Biotechnology and
382 Biological Sciences Research Council (BBSRC) grants BB/J014443/1 (B.S.), BB/K000659/1
383 (A.N.C), and BB/J011819/1 (P.W.A.D.). Funding from the European Research Council under
384 the European Union's Seventh Framework Programme grant FP7.2007-2013/grant

385 agreement number 322408 (A.E.A., D.J.B. and S.E.R) is also acknowledged. The Waters
386 Synapt G1 and G2-Si mass spectrometers were purchased with funding from the BBSRC
387 (BB/E012558/1 and BB/M012573/1, respectively). This project made use of time on the
388 ARC2 supercomputer facility at the University of Leeds, and time on ARCHER granted via
389 the UK High-End Computing Consortium for Biomolecular Simulation, HECBioSim
390 (www.hecbiosim.ac.uk), supported by the EPSRC (grant no. EP/L000253/1).

391

392 **Author contributions**

393 B.S. and A.N.C. contributed equally to this work. B.S. designed and performed the kinetic
394 experiments, computer modelling and molecular dynamics simulations. A.N.C. designed and
395 performed the mass-spectrometry and cross-linking experiments. P.W.A.D. designed and
396 performed *in vacuo* apo-Skp simulations. S.A.H. assisted and supervised the molecular
397 dynamics simulations. A.E.A, D.J.B. and S.E.R conceived, designed and supervised the
398 research. All authors contributed to discussion and were involved in editing the final
399 manuscript.

400

401 **Competing Financial Interests Statement**

402 The authors declare no competing financial interests.

403

404

405 **References for main text**

- 406 1. McMorran, L.M., Brockwell, D.J. & Radford, S.E. Mechanistic studies of the biogenesis and
 407 folding of outer membrane proteins *in vitro* and *in vivo*: What have we learned to date? *Arch*
 408 *Biochem Biophys* **564**, 265-280 (2014).
- 409 2. Kim, K.H., Aulakh, S. & Paetzel, M. The bacterial outer membrane beta-barrel assembly
 410 machinery. *Protein Sci* **21**, 751-68 (2012).
- 411 3. Hagan, C.L., Silhavy, T.J. & Kahne, D. beta-Barrel membrane protein assembly by the Bam
 412 complex. *Annu Rev Biochem* **80**, 189-210 (2011).
- 413 4. Voulhoux, R., Bos, M.P., Geurtsen, J., Mols, M. & Tommassen, J. Role of a highly conserved
 414 bacterial protein in outer membrane protein assembly. *Science* **299**, 262-5 (2003).
- 415 5. Ruiz, N., Kahne, D. & Silhavy, T.J. Advances in understanding bacterial outer-membrane
 416 biogenesis. *Nat Rev Microbiol* **4**, 57-66 (2006).
- 417 6. Sklar, J.G., Wu, T., Kahne, D. & Silhavy, T.J. Defining the roles of the periplasmic chaperones
 418 SurA, Skp, and DegP in *Escherichia coli*. *Genes Dev* **21**, 2473-84 (2007).
- 419 7. Goemans, C., Denoncin, K. & Collet, J.F. Folding mechanisms of periplasmic proteins. *Biochim*
 420 *Biophys Acta* **1843**, 1517-28 (2014).
- 421 8. Hartl, F.U., Bracher, A. & Hayer-Hartl, M. Molecular chaperones in protein folding and
 422 proteostasis. *Nature* **475**, 324-32 (2011).
- 423 9. Walton, T.A., Sandoval, C.M., Fowler, C.A., Pardi, A. & Sousa, M.C. The cavity-chaperone Skp
 424 protects its substrate from aggregation but allows independent folding of substrate domains.
 425 *Proc Natl Acad Sci U S A* **106**, 1772-7 (2009).
- 426 10. Walton, T.A. & Sousa, M.C. Crystal structure of Skp, a prefoldin-like chaperone that protects
 427 soluble and membrane proteins from aggregation. *Mol Cell* **15**, 367-74 (2004).
- 428 11. Korndorfer, I.P., Dommel, M.K. & Skerra, A. Structure of the periplasmic chaperone Skp
 429 suggests functional similarity with cytosolic chaperones despite differing architecture. *Nat*
 430 *Struct Mol Biol* **11**, 1015-20 (2004).
- 431 12. Jarchow, S., Luck, C., Gorg, A. & Skerra, A. Identification of potential substrate proteins for
 432 the periplasmic *Escherichia coli* chaperone Skp. *Proteomics* **8**, 4987-94 (2008).
- 433 13. Qu, J., Mayer, C., Behrens, S., Holst, O. & Kleinschmidt, J.H. The trimeric periplasmic
 434 chaperone Skp of *Escherichia coli* forms 1:1 complexes with outer membrane proteins via
 435 hydrophobic and electrostatic interactions. *J Mol Biol* **374**, 91-105 (2007).
- 436 14. Moon, C.P., Zaccai, N.R., Fleming, P.J., Gessmann, D. & Fleming, K.G. Membrane protein
 437 thermodynamic stability may serve as the energy sink for sorting in the periplasm. *Proc Natl*
 438 *Acad Sci U S A* **110**, 4285-90 (2013).
- 439 15. Burmann, B.M., Wang, C. & Hiller, S. Conformation and dynamics of the periplasmic
 440 membrane-protein-chaperone complexes OmpX-Skp and tOmpA-Skp. *Nat Struct Mol Biol* **20**,
 441 1265-72 (2013).
- 442 16. Callon, M., Burmann, B.M. & Hiller, S. Structural mapping of a chaperone-substrate
 443 interaction surface. *Angew Chem Int Ed Engl* **53**, 5069-72 (2014).
- 444 17. Bulieris, P.V., Behrens, S., Holst, O. & Kleinschmidt, J.H. Folding and insertion of the outer
 445 membrane protein OmpA is assisted by the chaperone Skp and by lipopolysaccharide. *J Biol*
 446 *Chem* **278**, 9092-9 (2003).
- 447 18. Lyu, Z.X., Shao, Q., Gao, Y.Q. & Zhao, X.S. Direct observation of the uptake of outer
 448 membrane proteins by the periplasmic chaperone Skp. *PLoS One* **7**, e46068 (2012).
- 449 19. Kleinschmidt, J.H. Membrane protein folding on the example of outer membrane protein A
 450 of *Escherichia coli*. *Cell Mol Life Sci* **60**, 1547-58 (2003).
- 451 20. Bishop, R.E. The lipid A palmitoyltransferase PagP: molecular mechanisms and role in
 452 bacterial pathogenesis. *Mol Microbiol* **57**, 900-12 (2005).
- 453 21. Vandeputte-Rutten, L. et al. Crystal structure of the outer membrane protease OmpT from
 454 *Escherichia coli* suggests a novel catalytic site. *EMBO J* **20**, 5033-9 (2001).

- 455 22. Yamashita, E., Zhalnina, M.V., Zakharov, S.D., Sharma, O. & Cramer, W.A. Crystal structures
456 of the OmpF porin: function in a colicin translocon. *EMBO J* **27**, 2171-80 (2008).
- 457 23. Noinaj, N., Rollauer, S.E. & Buchanan, S.K. The beta-barrel membrane protein insertase
458 machinery from Gram-negative bacteria. *Curr Opin Struct Biol* **31**, 35-42 (2015).
- 459 24. Otzen, D.E. & Andersen, K.K. Folding of outer membrane proteins. *Arch Biochem Biophys* **531**,
460 34-43 (2013).
- 461 25. Burgess, N.K., Dao, T.P., Stanley, A.M. & Fleming, K.G. Beta-barrel proteins that reside in the
462 *Escherichia coli* outer membrane *in vivo* demonstrate varied folding behavior *in vitro*. *J Biol*
463 *Chem* **283**, 26748-58 (2008).
- 464 26. Heller, K.B. Apparent molecular weights of a heat-modifiable protein from the outer
465 membrane of *Escherichia coli* in gels with different acrylamide concentrations. *J Bacteriol*
466 **134**, 1181-3 (1978).
- 467 27. McMorran, L.M., Bartlett, A.I., Huysmans, G.H., Radford, S.E. & Brockwell, D.J. Dissecting the
468 effects of periplasmic chaperones on the *in vitro* folding of the outer membrane protein
469 PagP. *J Mol Biol* **425**, 3178-91 (2013).
- 470 28. Ruotolo, B.T., Benesch, J.L., Sandercock, A.M., Hyung, S.J. & Robinson, C.V. Ion mobility-mass
471 spectrometry analysis of large protein complexes. *Nat Protoc* **3**, 1139-52 (2008).
- 472 29. Hernandez, H. & Robinson, C.V. Determining the stoichiometry and interactions of
473 macromolecular assemblies from mass spectrometry. *Nat Protoc* **2**, 715-26 (2007).
- 474 30. Ruotolo, B.T. et al. Evidence for macromolecular protein rings in the absence of bulk water.
475 *Science* **310**, 1658-61 (2005).
- 476 31. Burmann, B.M., Holdbrook, D.A., Callon, M., Bond, P.J. & Hiller, S. Revisiting the interaction
477 between the chaperone Skp and lipopolysaccharide. *Biophys J* **108**, 1516-26 (2015).
- 478 32. Sandlin, C.W., Zaccai, N.R. & Fleming, K.G. Skp trimer formation is insensitive to salts in the
479 physiological range. *Biochemistry* **54**, 7059-7062 (2015).
- 480 33. Bush, M.F. et al. Collision cross sections of proteins and their complexes: a calibration
481 framework and database for gas-phase structural biology. *Anal Chem* **82**, 9557-65 (2010).
- 482 34. Ruotolo, B.T. & Robinson, C.V. Aspects of native proteins are retained in vacuum. *Curr Opin*
483 *Chem Biol* **10**, 402-8 (2006).
- 484 35. Zaccai, N.R. et al. Deuterium labeling together with contrast variation small-angle neutron
485 scattering suggests how Skp captures and releases unfolded outer membrane proteins.
486 *Methods Enzymol* **566**, 159-210 (2016).
- 487 36. Marklund, E.G., Degiacomi, M.T., Robinson, C.V., Baldwin, A.J. & Benesch, J.L. Collision cross
488 sections for structural proteomics. *Structure* **23**, 791-9 (2015).
- 489 37. Siegert, R., Leroux, M.R., Scheufler, C., Hartl, F.U. & Moarefi, I. Structure of the molecular
490 chaperone prefoldin: unique interaction of multiple coiled coil tentacles with unfolded
491 proteins. *Cell* **103**, 621-32 (2000).
- 492 38. Schwalm, J., Mahoney, T.F., Soltes, G.R. & Silhavy, T.J. Role for Skp in LptD assembly in
493 *Escherichia coli*. *J Bacteriol* **195**, 3734-42 (2013).
- 494 39. Thoma, J., Burmann, B.M., Hiller, S. & Muller, D.J. Impact of holdase chaperones Skp and
495 SurA on the folding of beta-barrel outer-membrane proteins. *Nat Struct Mol Biol* **22**, 795-802
496 (2015).
- 497 40. Burmann, B.M. & Hiller, S. Chaperones and chaperone-substrate complexes: Dynamic
498 playgrounds for NMR spectroscopists. *Prog Nucl Magn Reson Spectrosc* **86-87**, 41-64 (2015).
- 499 41. Quan, S. et al. Super Spy variants implicate flexibility in chaperone action. *Elife* **3**, e01584
500 (2014).
- 501 42. Stirling, P.C., Bakhoun, S.F., Feigl, A.B. & Leroux, M.R. Convergent evolution of clamp-like
502 binding sites in diverse chaperones. *Nat Struct Mol Biol* **13**, 865-70 (2006).

- 503 43. Harms, N. et al. The early interaction of the outer membrane protein phoe with the
504 periplasmic chaperone Skp occurs at the cytoplasmic membrane. *J Biol Chem* **276**, 18804-11
505 (2001).
- 506 44. Robert, V. et al. Assembly factor Omp85 recognizes its outer membrane protein substrates
507 by a species-specific C-terminal motif. *PLoS Biol* **4**, e377 (2006).
- 508 45. Estrada Mallarino, L. et al. TtOmp85, a beta-barrel assembly protein, functions by barrel
509 augmentation. *Biochemistry* **54**, 844-52 (2015).
- 510 46. Hagan, C.L., Wzorek, J.S. & Kahne, D. Inhibition of the beta-barrel assembly machine by a
511 peptide that binds BamD. *Proc Natl Acad Sci U S A* **112**, 2011-2016 (2015).
- 512 47. Patel, G.J. & Kleinschmidt, J.H. The lipid bilayer-inserted membrane protein BamA of
513 *Escherichia coli* facilitates insertion and folding of outer membrane protein A from its
514 complex with Skp. *Biochemistry* **52**, 3974-86 (2013).
- 515 48. Fleming, K.G. A combined kinetic push and thermodynamic pull as driving forces for outer
516 membrane protein sorting and folding in bacteria. *Philos Trans R Soc Lond B Biol Sci* **370**,
517 20150026 (2015).
- 518 49. Kim, Y.E., Hipp, M.S., Bracher, A., Hayer-Hartl, M. & Hartl, F.U. Molecular chaperone
519 functions in protein folding and proteostasis. *Annu Rev Biochem* **82**, 323-55 (2013).
- 520 50. Arora, A., Abildgaard, F., Bushweller, J.H. & Tamm, L.K. Structure of outer membrane protein
521 A transmembrane domain by NMR spectroscopy. *Nat Struct Biol* **8**, 334-8 (2001).
- 522 51. Ahn, V.E. et al. A hydrocarbon ruler measures palmitate in the enzymatic acylation of
523 endotoxin. *EMBO J* **23**, 2931-41 (2004).
- 524 52. Ni, D. et al. Structural and functional analysis of the beta-barrel domain of BamA from
525 *Escherichia coli*. *FASEB J* **28**, 2677-85 (2014).
- 526 53. Seshadri, K., Garemyr, R., Wallin, E., von Heijne, G. & Elofsson, A. Architecture of beta-barrel
527 membrane proteins: analysis of trimeric porins. *Protein Sci* **7**, 2026-32 (1998).
- 528

529

530

531

532

533 **Figure legends for main text**

534

535 **Figure 1: Three-dimensional structures of Skp and the OMPs used in this study (a)**

536 Skp (PDB 1U2M¹¹), (b) tOmpA (PDB:1G90⁵⁰), (c) PagP (PDB:1THQ⁵¹), (d) OmpT
537 (PDB:1I78²¹), (e) OmpF (PDB:2ZFG²²), and (f) tBamA (PDB 4N75⁵²). All structures are to
538 scale. OmpF is a functional trimer; for clarity only one subunit is colored and the other two
539 are shown in grey. Residues missing from chains B and C in the Skp crystal structure were
540 modelled from chain A (green). In (b)-(f) the OM is represented in pale green, and
541 approximate positions of OMPs within the membrane are judged by the position of residues
542 in the 'aromatic girdles' at either side of the membrane⁵³.

543

544 **Figure 2: Different Skp:OMP ratios are required to sequester OMPs and inhibit folding.**

545 Folding data for (a) tOmpA, (b) PagP, (c) OmpF, and (d) tBamA. Fluorescence emission
546 spectra (left) of OMPs folded in *d*C_{11:0}PC liposomes (red lines), unfolded in 8M urea (grey
547 lines), in buffer alone in the absence of lipids (purple lines), and in the presence of a 2-fold
548 molar excess of Skp (cyan lines). Final OMP concentrations were 0.4 μM, with a molar
549 lipid:protein ratio of 3200:1 (in folded samples), in 0.24 M urea, 50 mM glycine-NaOH, pH
550 9.5, at 25 °C. Kinetic traces (middle) for the folding of OMP alone into *d*C_{11:0}PC liposomes
551 (red lines), and in the presence of Skp at a 1:1 molar ratio (trimer equivalents, see Methods)
552 (tOmpA and PagP, green lines, parts (a) and (b)), a 2:1 molar ratio (cyan lines, parts (a)–(d)),
553 a 4:1 molar ratio (OmpF and tBamA, orange lines, parts (c) and (d)), or in the absence of
554 lipids (purple lines). Single or double exponential fits to the data (see Supplementary Table
555 2) are shown as dotted lines. Rate constants for OMP folding in the absence or presence of
556 Skp at the OMP:Skp ratio indicated (right). Where the data were best described by a double
557 exponential fit, the rate constants for the second, slower, phase are not shown (see
558 **Supplementary Table 2** for full details). A star indicates a Skp:OMP ratio where folding did

559 not occur on the timescale of these experiments. Data are shown as mean \pm standard
560 deviation of three independent experiments using three separate liposome batches.

561

562 **Figure 3: Skp:OMP complexes have different stoichiometries.** ESI mass spectra of (a)
563 Skp (5 μ M) and Skp pre-incubated in the presence of 5 μ M (b) tOmpA, (c) PagP, (d) OmpT,
564 (e) OmpF and (f) tBamA. Spectra are annotated with red circles (Skp), green squares (1:1
565 Skp:OMP) and blue triangles (2:1 Skp:OMP). The most abundant charge state is labelled for
566 each distribution. Observed masses for the complexes are summarized in **Supplementary**
567 **Table 3**. Complementary IMS data are displayed in **Supplementary Fig. 3**.

568

569 **Figure 4: Collision cross-section distributions of Skp and Skp:OMP complexes.** CCS
570 distributions (peak heights normalized to MS peak intensity) of (a) Skp and 1:1 Skp:OMP
571 complexes with (b) tOmpA, (c) PagP, (d) OmpT, (e) OmpF and (f) tBamA. The width at half
572 height (normalized for spectral intensity) for each distribution is indicated (dashed lines), as
573 well as the charge states which are represented by each CCS distribution. (g) Plot of
574 observed CCSs of the assemblies as a function of charge state (mean of three replicates
575 shown, note that standard deviation values are smaller than the symbol size used): Skp,
576 black squares; 1:1 Skp:tOmpA, red circles; 1:1 Skp:PagP, green circles; 1:1 Skp:OmpT,
577 orange circles; 1:1 Skp:OmpF, blue circles; 1:1 Skp:tBamA, purple circles; 2:1 Skp:OmpT,
578 orange open squares; 2:1 Skp:OmpF, blue open squares; 2:1 Skp:tBamA, purple open
579 squares. Dashed lines indicate CCSs estimated from (i) the collapsed structure of Skp from
580 the MD simulation (black) (**Supplementary Fig. 7e**), (ii) the crystal structure of Skp (red), (iii)
581 a model 1:1 Skp:OMP complex with an expanded central cavity (orange), (iv) a model 2:1
582 Skp:OMP complex comprising two interlocking Skp molecules (green) and (v) a model
583 (Skp)₂:OMP complex arranged in a side-by-side fashion (pink) (**Fig. 5**). (h) Plot of the lowest
584 measured CCS of each assembly as a function of molecular weight (symbols as in (g)). The

585 line represents the expected CCSs for globular proteins with an amino acid density of 0.33
586 Da.Å⁻³.

587

588 **Figure 5: Possible architectures of Skp:OMP complexes.** Side (left) and bottom (right)
589 view surface representations of models of (a) Skp (yellow) (based on the published crystal
590 structure (PDB: 1U2M¹⁰) with missing residues modelled by molecular replacement), bound
591 to an 8-stranded OMP represented by a grey sphere of radius 20 Å, (b) Skp with an
592 expanded central cavity surrounding a 16-stranded OMP represented by a grey sphere of
593 radius 25 Å, (c,d) 2:1 Skp:OMP structures (Skp colored in yellow and green) arranged side-
594 by-side in a (c) parallel or (d) antiparallel arrangement, with the 16-stranded OMP substrate
595 represented by a grey capsule with cylinder height of 37 Å and cap radii of 20 Å, (e) 2:1
596 Skp:OMP complex with an interlocked architecture with the 16-stranded OMP represented
597 by a grey sphere of radius 25 Å, and (f) the hexameric eukaryotic chaperone prefoldin (PDB:
598 1FXK³⁷), with chains A, B and C of the crystal structure shown in green, cyan and yellow,
599 respectively.

600

601 **Figure 6: *In vacuo* molecular dynamics simulations of 1:1 and 2:1 Skp-OMP**
602 **complexes.** (a) Starting model of a 1:1 Skp:tOmpA complex used for MD simulations
603 (**Supplementary Data Set 4**), and (b) the structure obtained after 10 ns of *in vacuo*
604 simulation (**Supplementary Data Set 5**). (c) Starting model of a 2:1 Skp:tBamA complex
605 used for MD simulations, with the two copies of Skp arranged in a side-by-side parallel
606 orientation (**Fig. 5c**) (**Supplementary Data Set 6**), and (d) the structure obtained after 10 ns
607 of *in vacuo* simulation (**Supplementary Data Set 7**). Views from the side (top row) and
608 bottom (bottom row) are shown. Skp (green/blue) is shown in cartoon representation. OMPs
609 (yellow) are shown in surface representation. Representative structures are shown from

610 three independent MD simulations, and CCS values in the text are the mean \pm standard
611 deviation of three MD simulations.

612

613 **Figure 7: Molecular dynamics simulations of 1:1 and 2:1 Skp:OMP complexes in**
614 **explicit solvent. (a)** Starting model of a 1:1 Skp:tOmpA complex used for MD simulations
615 (left) (**Supplementary Data Set 4**) and the structure obtained after 100 ns of simulation in
616 explicit solvent (right) (**Supplementary Data Set 8**). **(b)** Starting model of a 2:1 Skp:tBamA
617 complex used for MD simulations (left) (**Supplementary Data Set 6**), with the two copies of
618 Skp arranged in a side-by-side parallel orientation (**Fig. 5c**), and the structure obtained after
619 100 ns of simulation in explicit solvent (right) (**Supplementary Data Set 9**). **(c,d)** Backbone
620 RMSDs calculated for the 100 ns simulations of **(c)** 1:1 Skp:tOmpA, and **(d)** 2:1 Skp:tBamA
621 in explicit solvent, demonstrating that the complexes are stable over this timescale.
622 Representative structures are shown from three independent MD simulations, and CCS
623 values in the text are the mean \pm standard deviation of three MD simulations.

624

625 **Online Methods**

626 **Cloning of OmpF, tBamA and OmpT**

627 A codon optimized synthetic gene (Eurofins, Germany) of the mature sequence of OmpF
628 (residues 23-362) was cloned into pET11a (Novagen, UK) between the NdeI (5') and
629 BamHI (3') restriction sites. To create the tBamA construct, residues 425-810 of BamA were
630 amplified by PCR, using plasmid BamAB-pETDUET-1 (kindly donated by Dr Susan
631 Buchanan (NIH, USA)) as the template, and the resultant product then ligated into pET11a
632 as described above. The OmpT mature sequence (residues 21-217) was amplified by PCR
633 from *E. coli* XL1-blue cells to include an N-terminal 6xHis-tag and TEV protease cleavage
634 site (MH₆ENLYFQG-OmpT), and subsequently cloned into the pET11a vector as described
635 above. The plasmids for tOmpA, PagP, OmpA and BamA encoding the mature OMP
636 sequences were kindly provided by Dr Karen Fleming (John Hopkins University, USA)²⁵.

637

638 **Expression and purification of PagP, tOmpA, OmpF, tBamA, OmpA and BamA**

639 The relevant plasmid was transformed into BL21[DE3] cells (Stratagene, UK) and the
640 appropriate OMP was expressed and purified as previously described²⁷. Protein
641 concentrations were determined spectrophotometrically using molar extinction coefficients at
642 280 nm of 82,390, 46,870, 54,210, 101,315, 52,955 and 140,040 M⁻¹ cm⁻¹ for PagP, tOmpA,
643 OmpF, tBamA, OmpA and BamA, respectively.

644

645 **Expression and purification of OmpT**

646 Expression and purification for OmpT was carried out as previously described⁵⁴. Protein
647 concentration was determined spectrophotometrically using a molar extinction coefficient at
648 280 nm of 79,760 M⁻¹ cm⁻¹.

649

650 **Expression and purification of Skp**

651 The pET21b plasmid, containing the full-length Skp gene, including the N-terminal signal
652 sequence, was transformed into BL21[DE3] cells (Stratagene, UK). Cells were grown in LB
653 medium containing 100 µg/mL carbenicillin at 27 °C with shaking (200 rpm) until the culture
654 reached an OD₆₀₀ of ~0.6 (after ~6 h). Cultures were induced with 25 µM IPTG, expressed
655 overnight, and harvested by continuous centrifugation at 15000 rpm (Heraeus Contifuge,
656 Rotor 8575, Thermo Fisher Scientific, UK). The cell pellet was resuspended in 50 mM Tris-
657 HCl, 5 mM EDTA, 50 mM NaCl, pH 7.5 at 4 °C with gentle agitation for ~48 h. 1 mg/mL
658 polymyxin B sulphate was added to the resuspended cells, and then incubated for 1 h at
659 4 °C with gentle agitation. Spheroplasts were sedimented by centrifugation (12 000 *g*, 20
660 min 4 °C) and the supernatant dialyzed against 20 mM Tris-HCl, 100 mM NaCl, pH 8.0
661 (Buffer A) overnight at 4 °C. The periplasmic extract was filtered (0.4 µm syringe filter,
662 Sartorius, UK) and loaded onto a HiTrapQ (5 mL) anion exchange column (GE Healthcare,
663 UK). The flow through from this column was loaded onto a HiTrap SP (5 mL) cation
664 exchange column (GE Healthcare, UK) equilibrated with Buffer A. The column was washed
665 with 5 column volumes of Buffer A and eluted with a gradient (0-100 %) of 20 mM Tris-HCl,
666 750 mM NaCl, pH 8.0 (Buffer B). Peak fractions were dialysed against 20 mM Tris-HCl, pH
667 8.0 and concentrated to ~50 µM (trimer) using Vivaspin 20 (5 kDa MWCO) concentrators
668 (Sartorius, UK). Aliquots were snap-frozen in liquid nitrogen and stored at -80 °C. Protein
669 concentrations were determined using a bicinchoninic acid (BCA) assay (Thermo Fisher
670 Scientific, UK), according to the manufacturer's instructions.

671

672 **Expression and purification of His-tagged Skp**

673 His-tagged Skp was expressed and purified using a protocol adapted from Burmann *et al.*¹⁵.
674 The pET28b plasmid, containing the Skp gene with an N-terminal 6xHis-tag and thrombin
675 cleavage site, was transformed into BL21[DE3]pLysS cells (Stratagene, UK). Cells were

676 grown in LB medium containing 30 µg/mL kanamycin at 37 °C with shaking (200 rpm) until
677 the culture reached an OD₆₀₀ of ~0.6. The temperature was then lowered to 20 °C and
678 expression induced with 0.4 mM IPTG. Following overnight expression (~18 h) cells were
679 harvested by centrifugation, resuspended in 25 mM Tris-HCl, pH 7.2, 150 mM NaCl, 20 mM
680 imidazole, containing a cocktail of EDTA-free protease inhibitors (Roche), and lysed using a
681 cell disrupter (Constant Cell Disruption Systems, UK). Following centrifugation to remove
682 cell debris (20 mins, 4 °C, 39000 g), the lysate was applied to 5 mL HisTrap columns (GE
683 Healthcare) and washed with 25 mM Tris-HCl, pH 7.2, 150 mM NaCl, 20 mM imidazole.
684 His-tagged Skp was denatured on-column with 25 mM Tris-HCl, 6 M Gdn-HCl, pH 7.2, and
685 eluted with a 0-500 mM imidazole gradient over 50 mL in 25 mM Tris-HCl, 6 M Gdn-HCl, pH
686 7.2. Fractions containing Skp were pooled and the protein refolded by dialysis against 25
687 mM Tris-HCl, pH 7.2, 150 mM NaCl. Refolded His-tagged Skp was concentrated to ~50 µM
688 (trimer) using Vivaspin 20 (5 kDa MWCO) concentrators (Sartorius, UK), aliquoted, snap-
689 frozen in liquid nitrogen and stored at -80 °C. Protein concentrations were determined using
690 a bicinchoninic acid (BCA) assay (Thermo Fisher Scientific, UK), according to the
691 manufacturer's instructions.

692

693 **Preparation of liposomes**

694 1,2-diundecanoyl-*sn*-glycero-3-phosphocholine (*d*C_{11:0}PC) (DUPC) lipids were purchased
695 from Avanti Polar Lipids (Alabama, USA). DUPC was obtained as a powder, dissolved in a
696 80:20 chloroform:methanol mixture at 25 mg/mL, and stored at -20 °C until use. Appropriate
697 volumes were transferred to glass test tubes and an even lipid film was created by drying
698 with a gentle stream of nitrogen while being shaken moderately in a 42 °C water bath. Lipid
699 films were further dried in a vacuum desiccator for >3 h, followed by resuspension in 50 mM
700 glycine-NaOH, pH 9.5 to a concentration of 40 mM. Resuspended lipids were vortexed
701 briefly and allowed to stand for 30 min. After vortexing again, lipids were subjected to 5
702 freeze-thaw cycles using liquid nitrogen. Large Unilamellar Vesicles (LUVs) (100 nm) were

703 prepared by extruding the lipid suspension 11 times through a 0.1 μm polycarbonate
704 membrane (Nuclepore, New Jersey, USA) using a mini extruder (Avanti Polar Lipids,
705 Alabama, USA). Liposomes were stored at 4 $^{\circ}\text{C}$ and used within 48 h of preparation.

706

707 **Kinetic folding assays**

708 Kinetic measurements were carried out using a Quantum Master Fluorimeter (Photon
709 Technology International, UK) controlled by FelixGX software v4.3. For each experiment,
710 four separate samples were run in a four cell changer maintained at 25 $^{\circ}\text{C}$ by a peltier-
711 controlled temperature unit. Tryptophan fluorescence of samples was excited at a
712 wavelength of 295 nm, and fluorescence emission was monitored at 335 nm. 295 nm rather
713 than 280 nm was chosen as the excitation wavelength as this minimizes the fluorescence
714 intensity contribution from Skp, which contains tyrosine but no tryptophan residues. The
715 excitation slit widths were set to 0.4-0.6 nm and the emission slit widths were set to 5 nm.
716 The high emission:excitation slit width ratio was important to minimize photobleaching on the
717 experimental time-scale. OMPs were buffer exchanged from 25 mM Tris-HCl, 6 M Gdn-HCl,
718 pH 8.0 into 50 mM glycine-NaOH, 8 M urea, pH 9.5 using Zeba spin desalting columns
719 (Thermo Scientific, UK) and diluted to 80 μM . OMP folding reactions in the absence of Skp
720 were initiated by diluting OMPs manually from this 80 μM unfolded protein stock in 8 M urea
721 to a final concentration of 0.4 μM protein and 0.24 M urea in the presence of 1.28 mM DUPC
722 liposomes (a lipid:protein molar ratio (LPR) of 3200:1), in 50 mM glycine-NaOH, pH 9.5.
723 Stable folding of Skp in 0.24 M urea was verified by CD (data not shown). The final volume
724 for each sample was 500 μL . For Skp-OMP experiments, OMPs were pre-incubated with
725 Skp for approximately 1 min prior to addition of liposomes. OMPs were diluted and mixed
726 from an 80 μM stock in 8 M urea to a final concentration of 2.4 μM , in the presence the
727 appropriate molar ratio of Skp, in 0.24 M urea, 50 mM glycine-NaOH, pH 9.5 (no lipids). This
728 Skp-OMP stock was then further diluted 6x in presence of 1.28 mM DUPC in 0.24 M urea,

729 50 mM glycine-NaOH, pH 9.5 to begin the assay. The final volume for each sample was 540
730 μL . At the concentrations of Skp utilized here, Skp has been shown to be in a dynamic
731 equilibrium between folded monomer subunits and trimers³². All Skp concentrations referred
732 to here are trimer equivalents. For each experiment with a particular liposome batch, four
733 samples were measured concurrently. A minimum of three replicates were globally fitted
734 using IgorPro 6.0 (Wavemetrics, Oregon, USA) to extract rate constant(s), forcing the fits to
735 share the same rate constant(s). Transients were fitted either to a single exponential function:
736

$$y = A_1 \cdot e^{-k_1 t} + c$$

737 or to a double exponential function:

$$y = (A_1 \cdot e^{-k_1 t}) + (A_2 \cdot e^{-k_2 t}) + c$$

738 Where k_1 and k_2 are rate constants, A_1 and A_2 are their associated amplitudes, and c is a
739 constant. Transients were fitted to a double exponential function if a satisfactory fit was not
740 obtained to a single exponential function as judged by inspection of residuals. Experiments
741 were performed for each condition using three separate liposome batches, and reported
742 errors are the standard deviation of rate constants between liposome batches.

743 **Fluorescence emission spectra**

744 Fluorescence emission spectra were acquired on the same instrument as the kinetic assays
745 (above). Each spectrum was recorded from 305 nm to 400 nm in 1 nm increments, using an
746 excitation wavelength of 295 nm. All spectra were acquired at 25 °C and all samples
747 contained 50 mM glycine-NaOH, pH 9.5, in a sample volume of 500 μL . OMPs from an 80
748 μM stock in 8 M urea were diluted to a final concentration of 0.4 μM in the presence of a 2-
749 fold molar excess of Skp in 0.24 M urea, 8 M urea, or buffer alone in 0.24 M urea. Folded
750 samples were prepared by dilution of an 80 μM OMP stock to 0.4 μM in the presence of 1.28

751 mM DUPC liposomes (molar LPR 3200:1) in 0.24 M urea and incubated at 25 °C for ~1.5 h
752 prior to acquisition of the fluorescence emission spectra.

753

754 **Mass Spectrometry**

755 Skp:OMP complexes were prepared by rapid dilution of the denatured OMP (400 µM in 8 M
756 urea, 50 mM glycine-NaOH, pH 9.5) to a final concentration of 5 µM into a solution of Skp (5
757 µM in 50 mM glycine-NaOH, pH 9.5). The samples were then buffer exchanged into 200 mM
758 ammonium acetate, pH 10 using Zeba spin desalting columns (Thermo Scientific, UK)
759 immediately prior to MS analysis. nanoESI-IMS-MS spectra were acquired using a Synapt
760 HDMS mass spectrometer (Waters Corporation, UK) using platinum/gold-plated borosilicate
761 capillaries prepared in-house. Typical instrument parameters include: capillary voltage 1.2-
762 1.6 kV, cone voltage 40 V, trap collision voltage 6 V, transfer collision voltage 10 V, trap DC
763 bias 20 V, backing pressure 4.5 mBar, IMS gas pressure 0.5 mBar, travelling wave height 7
764 V, travelling wave velocity 250 ms⁻¹. Data were processed using MassLynx v4.1, Driftscope
765 2.5 (Waters Corporation, UK) and Massign⁵⁵. CCSs were estimated by a calibration
766 approach^{28,33,56} using arrival time data for ions with known CCSs (β-lactoglobulin A, avidin,
767 concanavilin A and yeast alcohol dehydrogenase, all Sigma Aldrich, UK). Estimated modal
768 CCSs are shown as mean ± standard deviation of three independent experiments.
769 Theoretical CCSs for globular proteins with a given effective gas phase density were
770 calculated according to published methods⁵⁷.

771

772 **Chemical cross-linking and SDS-PAGE analysis.**

773 Samples for chemical cross-linking were prepared by rapid dilution of the urea denatured
774 OMP into a Skp solution (in 20 mM HEPES pH 7.5, 150 mM NaCl) at 4 °C, so that the final
775 concentrations of Skp and OMPs were 20 µM in a final concentration of 0.24 M urea.

776 Samples were mixed for 2 min and centrifuged (20 min, 13,000 *g*, 4 °C) to remove
777 aggregated material. The supernatant was removed and bis(sulfosuccinimidyl)suberate (BS3)
778 (Thermo Scientific, UK) was added at a 50-fold molar excess over the Skp concentration.
779 Samples were incubated at room temperature for 30 min, before the addition of 250 mM
780 glycine pH 9.5. Samples were analyzed by SDS-PAGE and the gels stained with Coomassie
781 Blue (InstantBlue, Expedeon, UK), or the proteins transferred to a PVDF membrane and
782 immunoblotted with an anti-His-HRP conjugated antibody (catalogue no. 15165, Thermo
783 Scientific, UK).

784

785 Gel bands were excised, cut into 1 mm³ pieces, destained with 30 % ethanol and washed
786 with 50 % acetonitrile in 25 mM ammonium bicarbonate (10 min). The gel pieces were then
787 dehydrated with acetonitrile (5 min), and the residual volatile solvent removed by
788 evaporation. They were then rehydrated with a solution of trypsin (Promega, UK) (20 ng uL⁻¹
789 in 25 mM ammonium bicarbonate) and incubated at 37 °C for 18 hours. Peptides were
790 recovered by incubating the gel pieces with 60 % acetonitrile/5 % formic acid (x 3), and the
791 samples were then concentrated.

792

793 Peptides were analysed by means of data-dependent LC-MS/MS on a nanoAcquity LC
794 system interfaced to a Synapt G2-Si HDMS mass spectrometer (Waters Ltd., Wilmslow,
795 Manchester, UK). Peptides (1 µL) were injected onto an Acquity M-Class C18, 75 µm x 150
796 mm column (Waters Ltd., Wilmslow, Manchester, UK) and then separated by gradient
797 elution of 1-50 % solvent B (0.1 % (v/v) formic acid in acetonitrile) in solvent A (0.1 % (v/v)
798 formic acid in water) over 60 min at 0.3 µL min⁻¹. Mass calibration was performed by a
799 separate injection of aqueous sodium iodide at a concentration of 2 µg/µl. [Glu1]-
800 Fibrinopeptide B was infused as a lock mass calibrant. Data acquisition was achieved using

801 data dependent analysis with a one second MS scan over an m/z range of 350-2000 being
802 followed by four 0.5 second MS/MS scans taken of the four most intense ions in the MS
803 spectrum. Data processing was performed using PEAKS Studio 7 (Bioinformatics Solutions,
804 Ontario, Canada).

805

806 **Modelling of Skp-OMP complexes**

807 All modelling was performed with the PyMOL Molecular Graphics System (v1.7rc1). To
808 generate models of the Skp:OMP complexes, the missing residues in chains B and C of the
809 Skp crystal structure (PDB: 1U2M¹⁰) were modelled from chain A. For the Skp:tOmpA/PagP
810 model (**Fig. 5a**) the OMP was modelled as a sphere of radius 20 Å with its origin positioned
811 at the geometric center between the α -carbon atoms of residue 50 of each Skp chain. For
812 the Skp:OMP model with expanded Skp subunits (**Fig. 5b**), each chain was positioned
813 around a sphere of radius 25 Å representing the larger OMP. The flexible tips of each
814 subunit (residues 51-101) were modelled hinged slightly inwards to wrap around the
815 substrate. The side-by-side parallel and antiparallel 2:1 Skp:OMP models (**Fig. 5c,d**) were
816 created by duplication of the Skp:tOmpA/PagP model (**Fig. 5a**) and appropriate rotation and
817 translation. The interlocking trimer 2:1 Skp:OMP model (**Fig. 5e**) was generated by
818 duplication of the Skp model with expanded subunits (**Fig. 5b**) and appropriate rotation and
819 translation of the duplicated Skp. Theoretical CCS values were generated using the
820 calibrated trajectory method implemented in the software IMPACT³⁶.

821

822 **Molecular Dynamics Simulations**

823 Molecular dynamics (MD) simulations were prepared using the AmberTools 14 suite of
824 programs, and performed using AMBER and the ff14SB forcefield⁵⁸. To simulate apo-Skp in
825 water, a Skp model was first generated from the Skp crystal structure (PDB: 1U2M¹⁰) with

826 the residues absent in chains B and C modelled from chain A. Following addition of
827 hydrogen atoms using xleap, Skp was placed in a TIP3P water box with a 10.0 Å cutoff and
828 the system neutralized with a total of 15 Cl⁻ ions. The system was equilibrated by performing
829 an initial energy minimization, followed by 80 ps of restrained MD during which the system
830 was heated to 300 K with gradual releasing of restraints. This was followed by an
831 unrestrained MD simulation of 100 ns.

832

833 Simulations of the collapse of the extended chains of tOmpA and tBamA were carried out
834 using a Generalized Born/Solvent Accessible surface area (GB/SA) implicit solvent
835 model^{59,60}. Use of an implicit solvent model speeds up exploration of conformational space
836 by at least an order of magnitude due to the neglect of frictional forces from collisions with
837 water molecules⁶¹, leading to rapid adoption of a collapsed configuration from the initially
838 linear structure (**Supplementary Fig. 7d, e, Supplementary Video 2**). The polypeptide
839 starting structures were generated in xleap and, after initial energy minimization, were
840 simulated for 3 ns. The starting models for the simulation of Skp-tOmpA and Skp₂-tBamA *in*
841 *vacuo* were created in PyMol by positioning OMPs, after simulated collapse, within the cavity
842 of Skp trimer structures in an 'open' conformation taken from the explicit solvent apo-Skp
843 simulation. All simulations except apo-Skp in explicit water were performed in triplicate. Each
844 *in vacuo* simulation of Skp-tOmpA and 2:1 Skp:tBamA was performed using a starting OMP
845 structure from a different simulation. *In vacuo* simulations of apo-Skp were performed using
846 three different starting structures selected from the simulation of apo-Skp in explicit water.
847 For all *in vacuo* simulations the system was equilibrated by performing an initial energy
848 minimization, followed by eight steps of restrained MD during which the system was heated
849 to 300 K with gradual releasing of restraints. This was followed by an unrestrained MD
850 simulation of 100 ns.

851

852 To simulate the 1:1 Skp:tOmpA and 2:1 Skp:tBamA complexes in solution, starting models
853 were generated as detailed above for the *in vacuo* simulations. The Skp:OMP complexes
854 were placed in a TIP3P water box with a 10.0 Å cutoff and the system neutralized with a total
855 of 10 Cl⁻ ions (1:1 Skp:tOmpA) or 12 Cl⁻ ions (2:1 Skp:tBamA). The systems were
856 equilibrated by performing an initial energy minimization, followed by 80 ps of restrained MD
857 during which the system was heated to 300 K with gradual releasing of restraints. This was
858 followed by an unrestrained MD simulation of 100 ns. For each complex simulations were
859 repeated in triplicate.

860

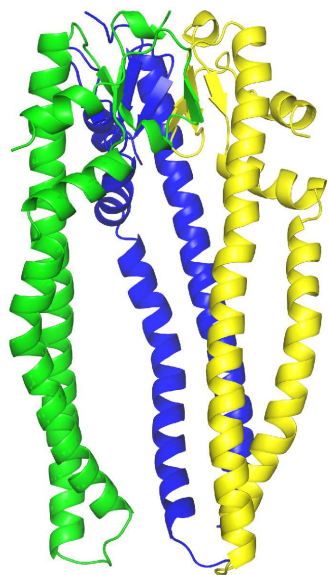
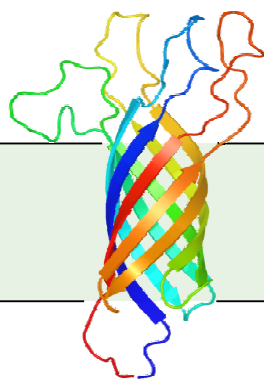
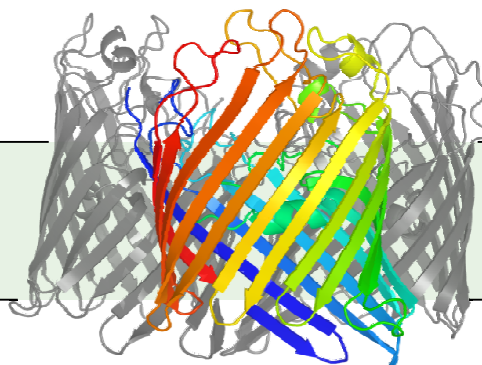
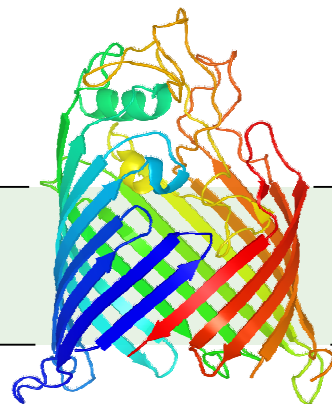
861 For comparison with IMS-MS data, theoretical collision cross-sections (CCSs) of final
862 structures at the end of simulations were calculated using the trajectory method and the
863 software IMPACT³⁶. CCS values for all structures following *in vacuo* simulations were
864 obtained after 100 ns of unrestrained simulation. CCS values for tOmpA and tBamA in
865 implicit solvent were obtained after 3 ns of unrestrained simulation. The integration time-step
866 was 2 fs and atomic positions were saved every 500 steps (1 ps). The software VMD was
867 used to compute backbone root mean square deviation (RMSD) and to render videos of the
868 simulations. Analysis of radius of gyration changes over trajectories were carried out with
869 ptraj.

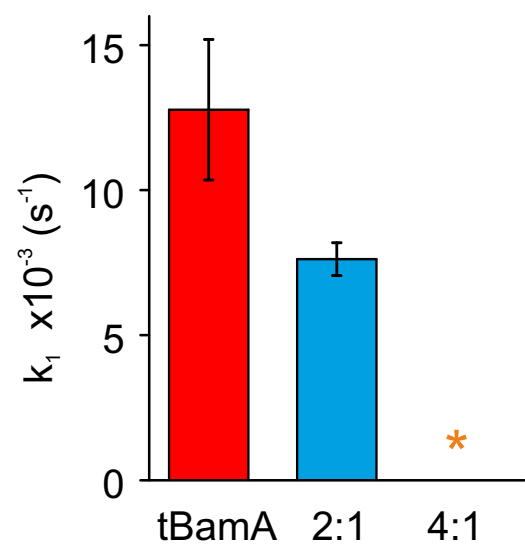
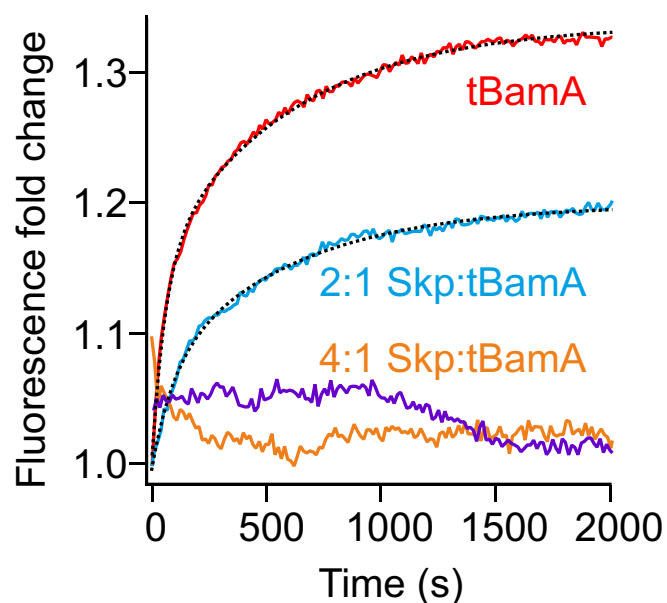
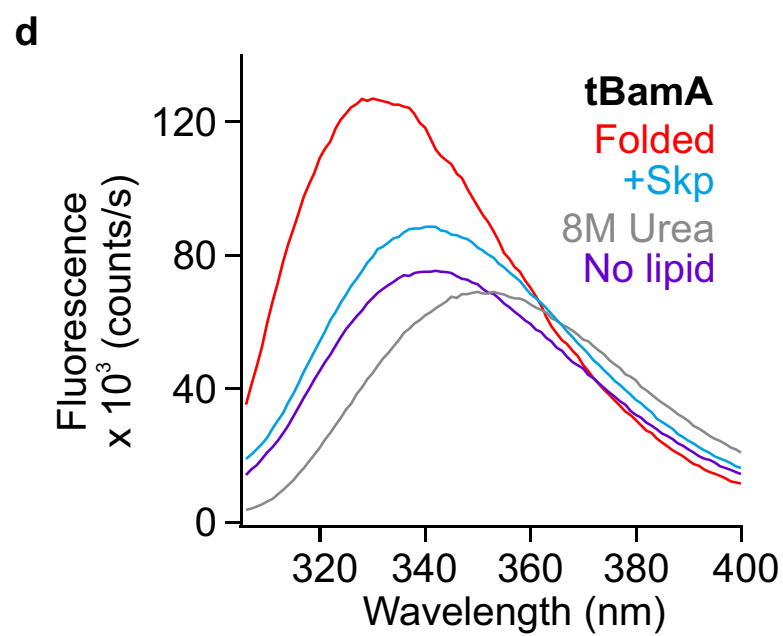
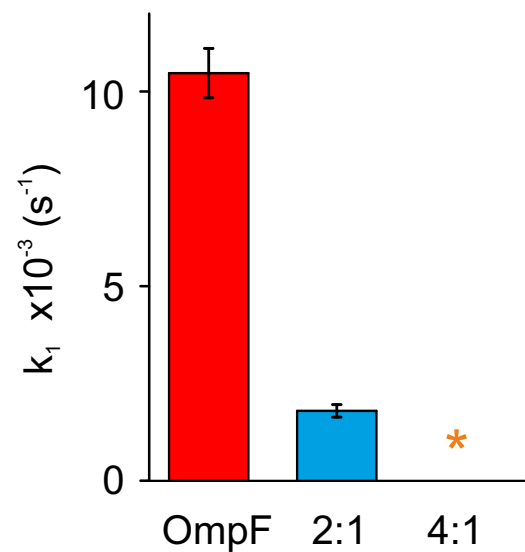
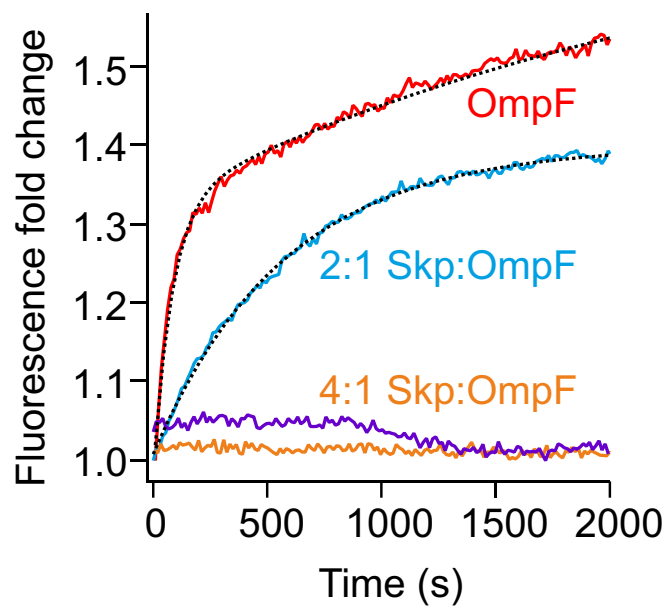
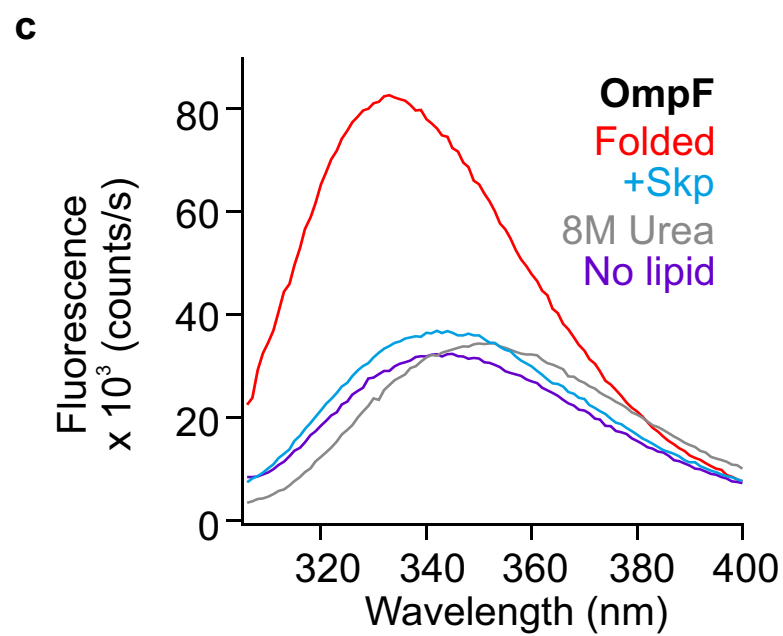
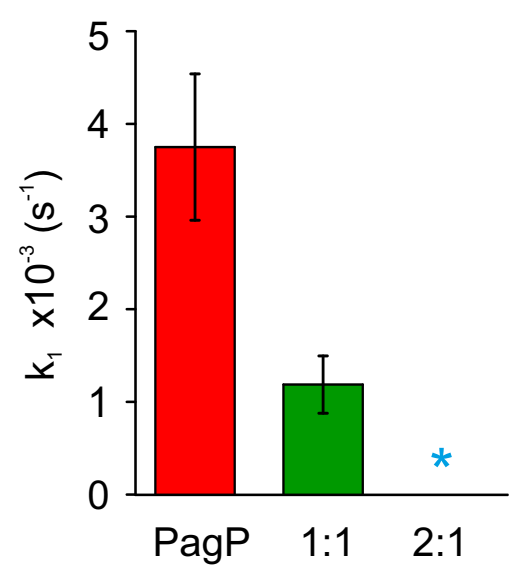
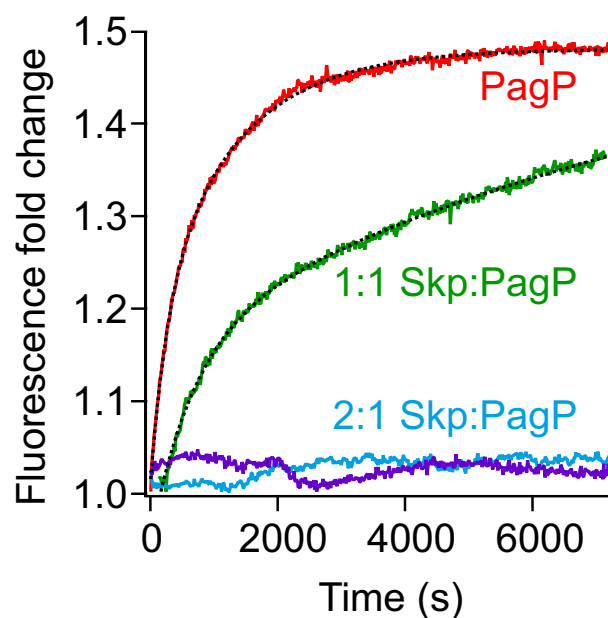
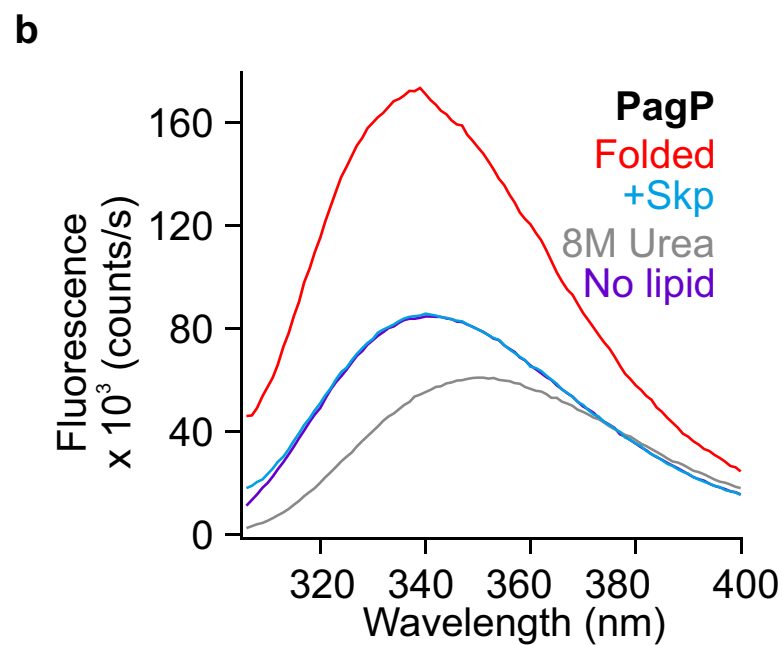
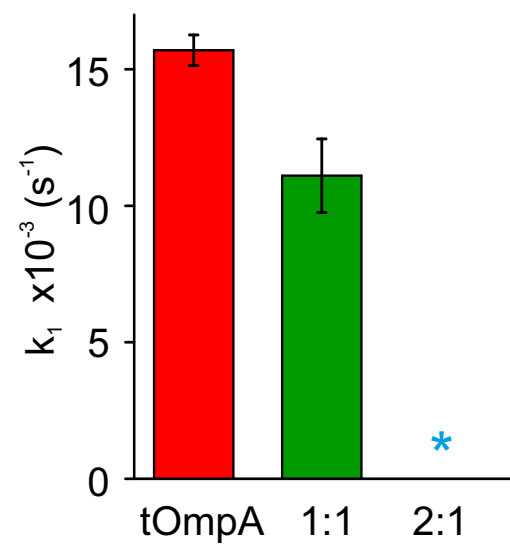
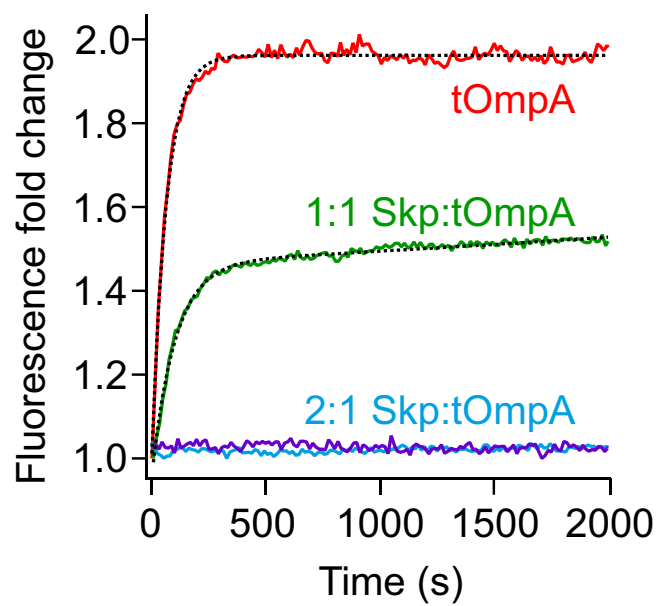
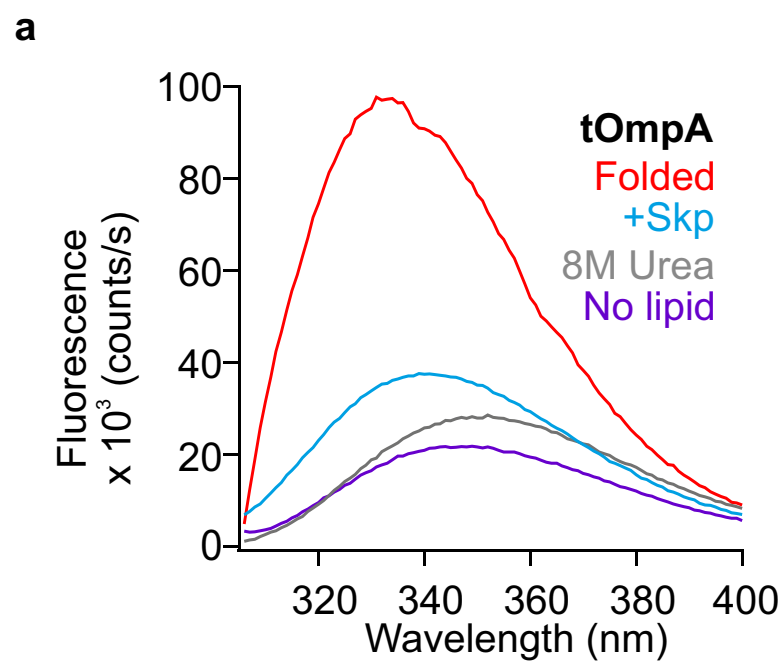
870

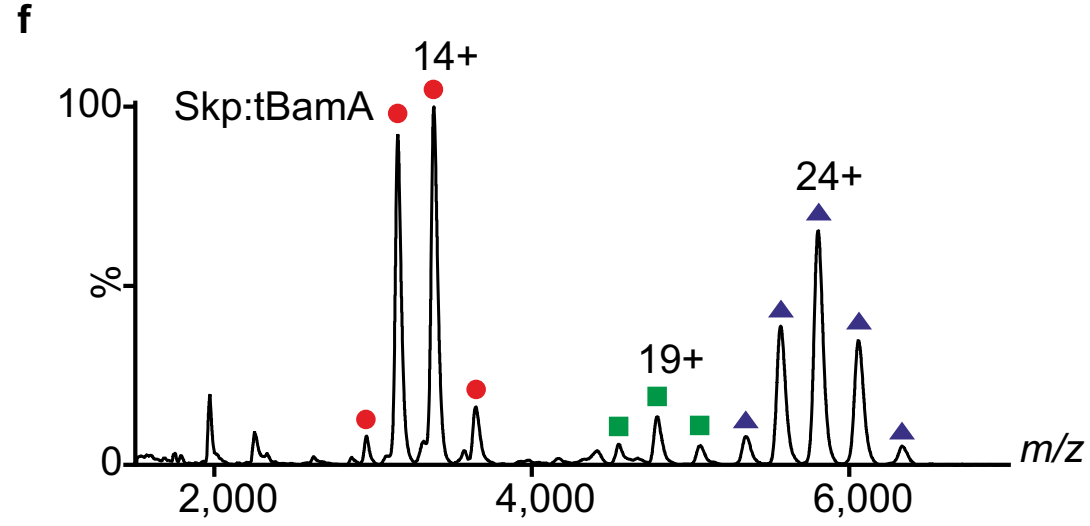
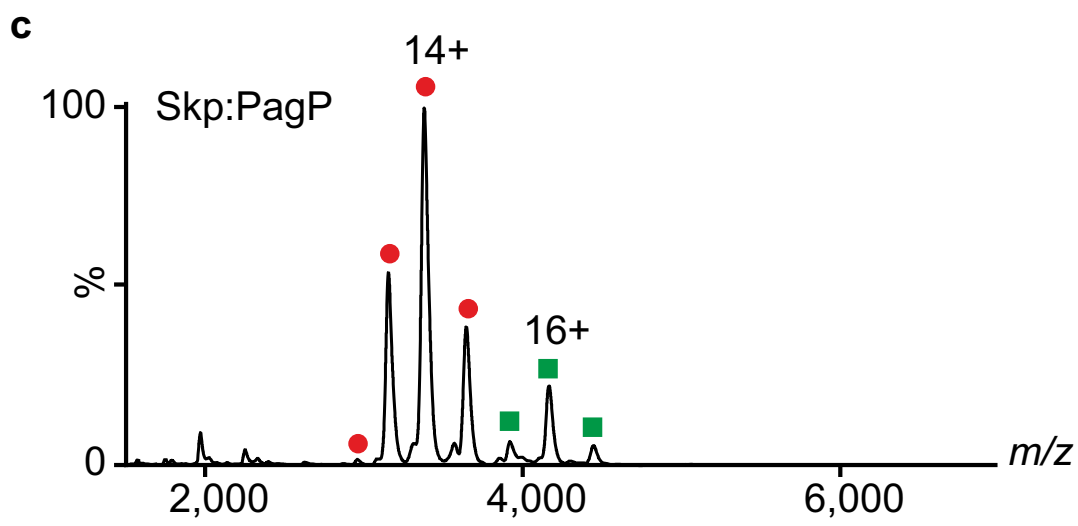
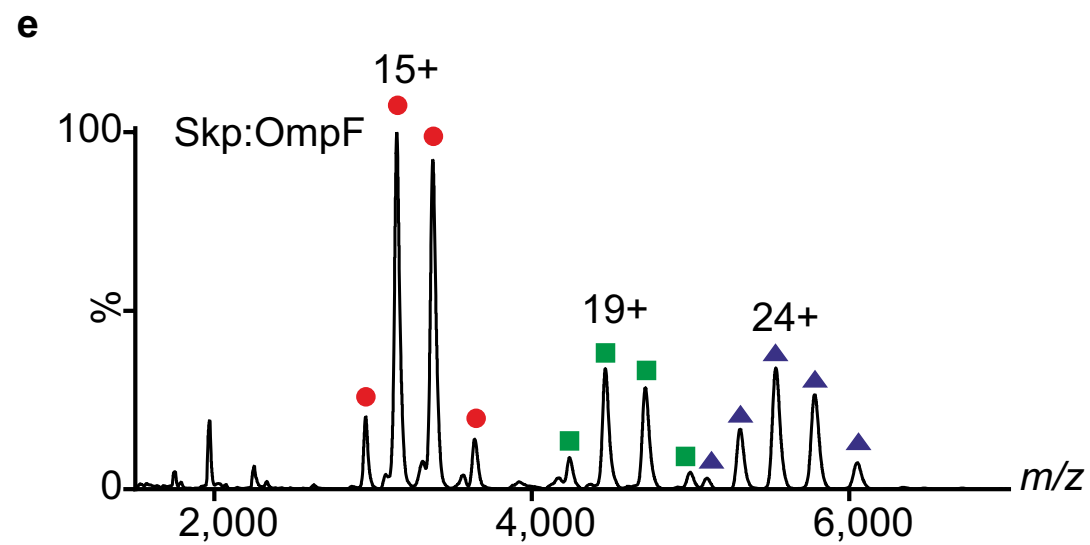
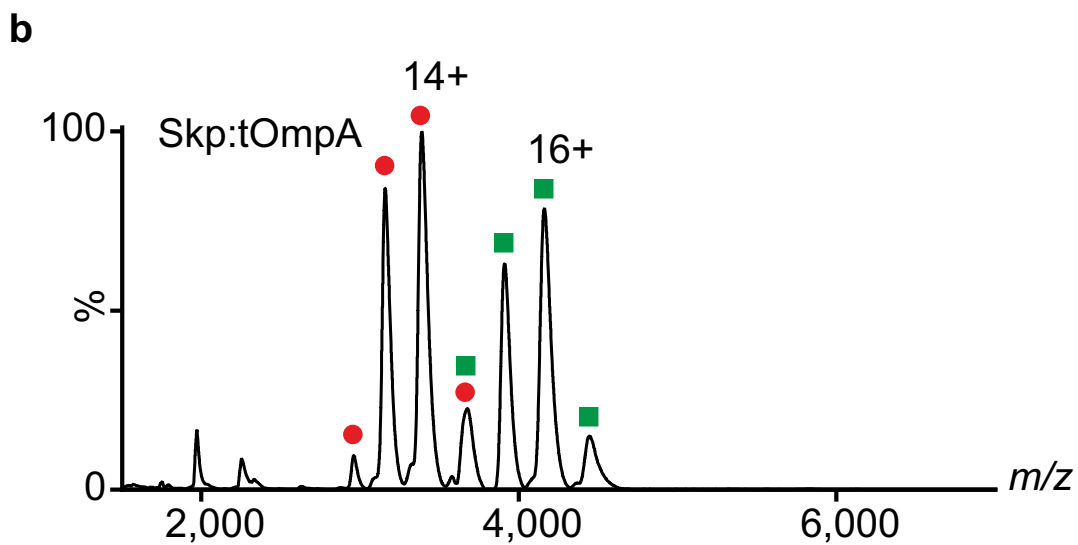
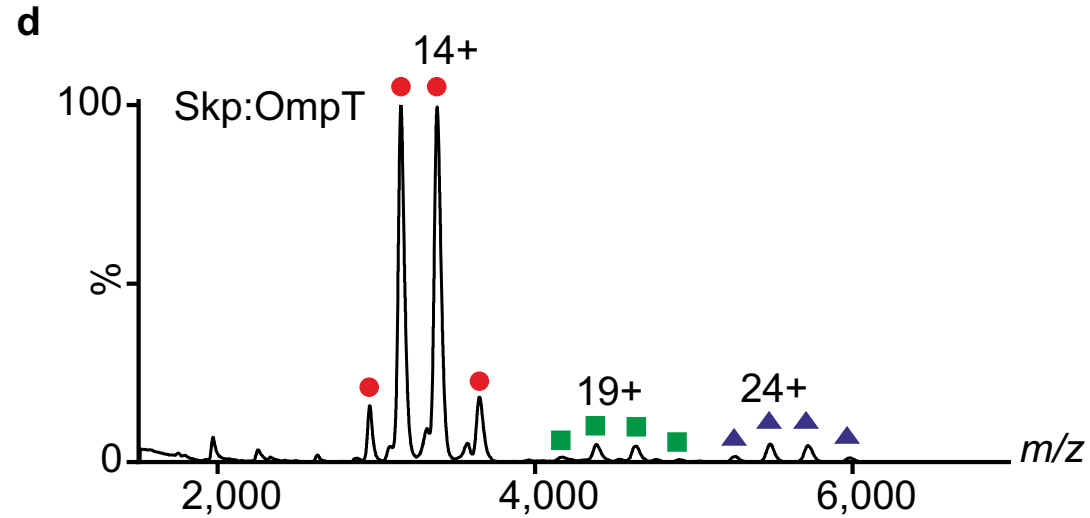
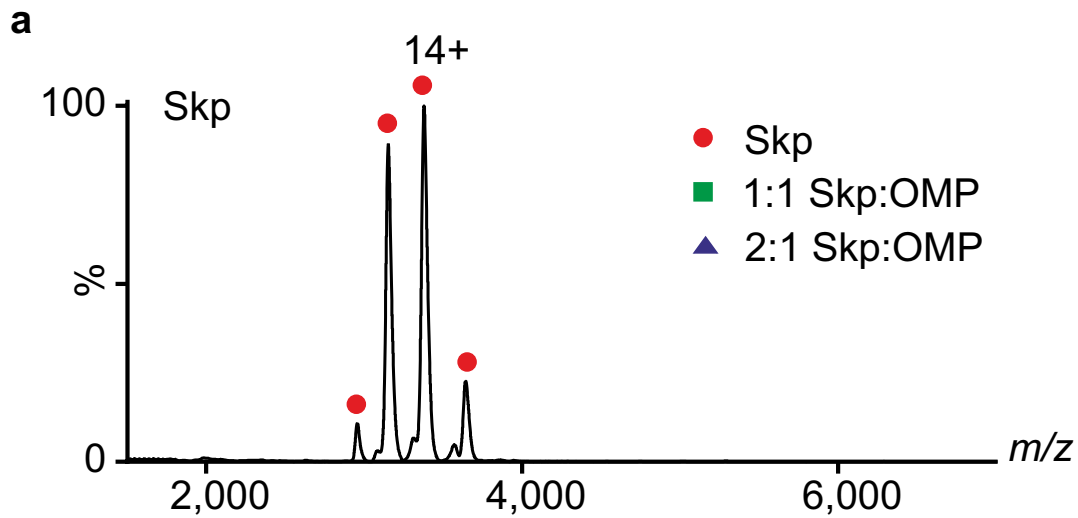
871 **Methods-only references**

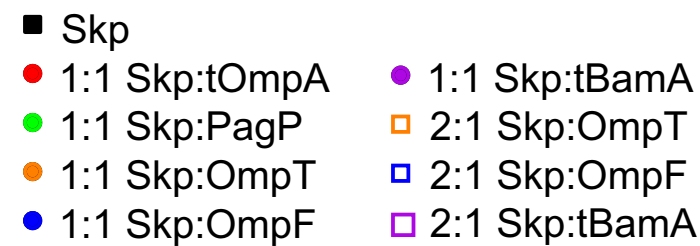
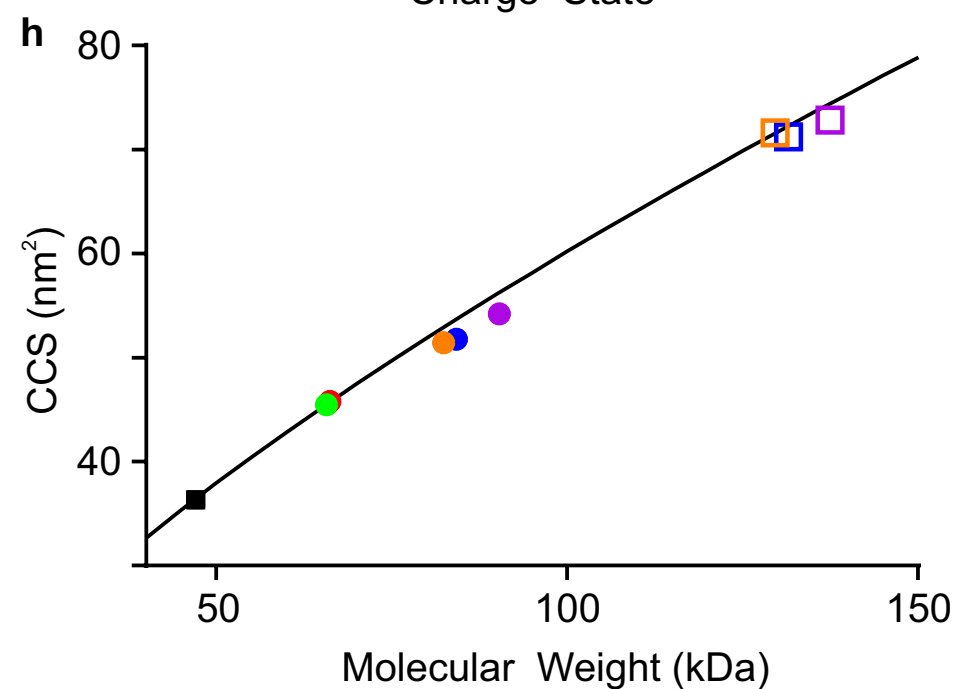
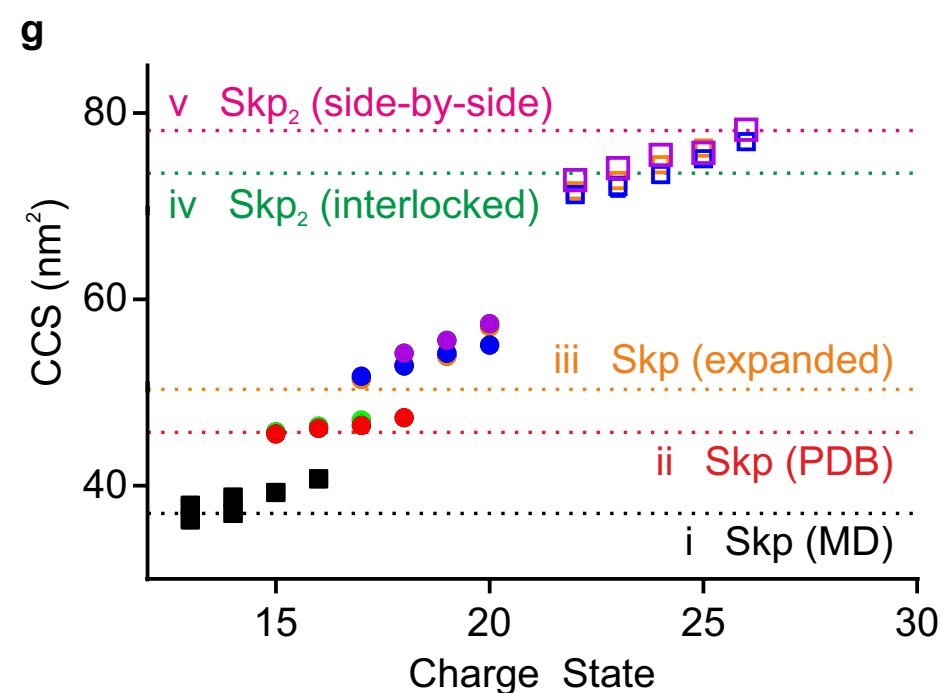
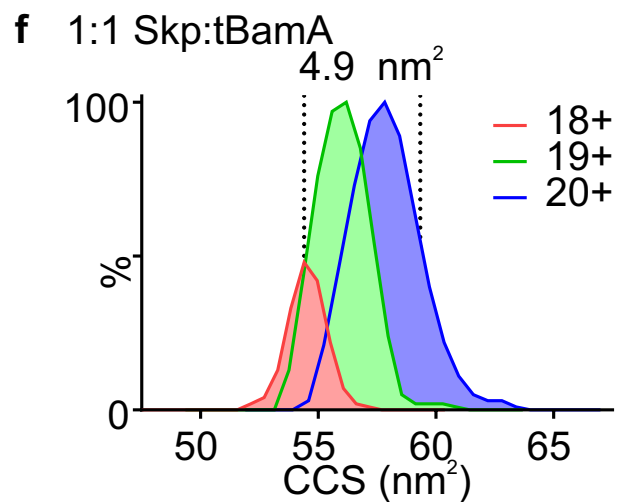
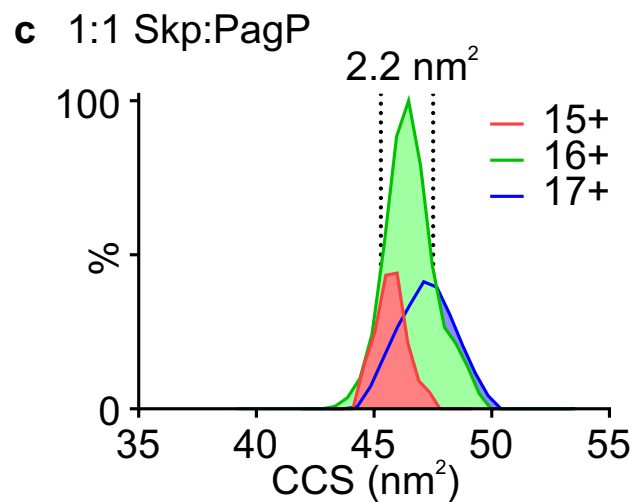
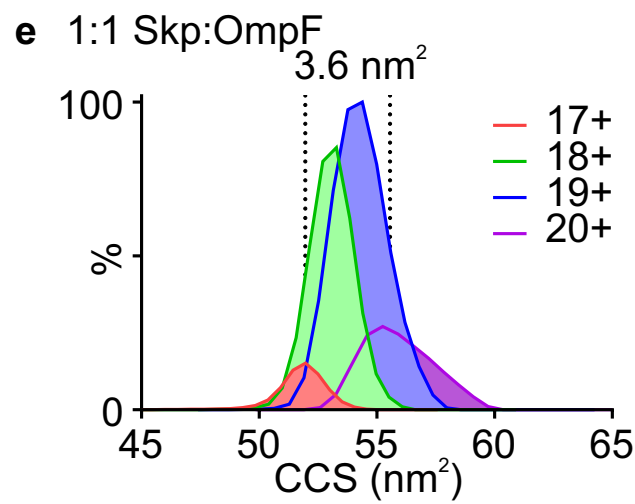
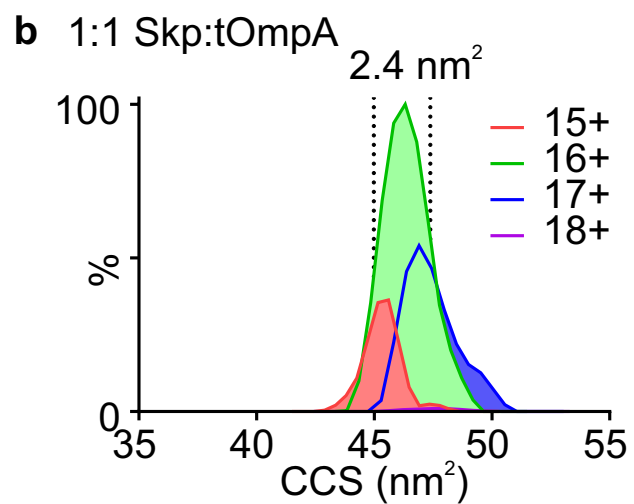
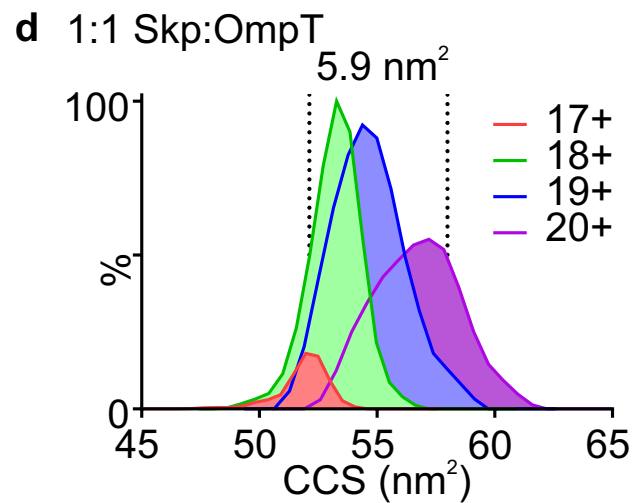
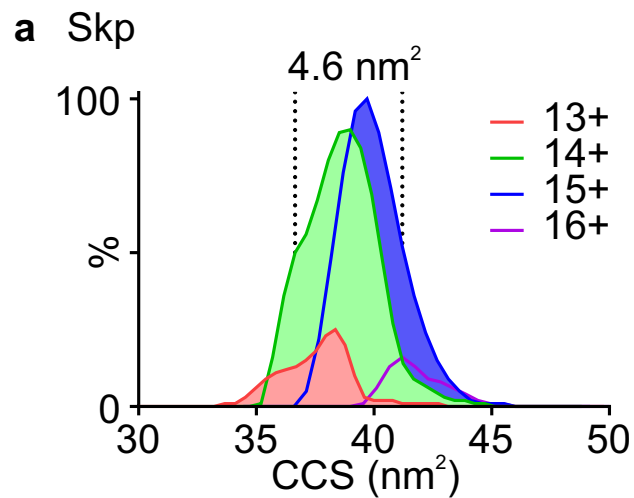
- 872 54. Calabrese, A.N., Watkinson, T.G., Henderson, P.J., Radford, S.E. & Ashcroft, A.E. Amphipols
873 outperform dodecylmaltoside micelles in stabilizing membrane protein structure in the gas
874 phase. *Anal Chem* **87**, 1118-26 (2015).
- 875 55. Morgner, N. & Robinson, C.V. Massign: an assignment strategy for maximizing information
876 from the mass spectra of heterogeneous protein assemblies. *Anal Chem* **84**, 2939-48 (2012).
- 877 56. Smith, D.P. et al. Deciphering drift time measurements from travelling wave ion mobility
878 spectrometry-mass spectrometry studies. *Eur J Mass Spectrom* **15**, 113-30 (2009).
- 879 57. Benesch, J.L., Ruotolo, B.T., Simmons, D.A. & Robinson, C.V. Protein complexes in the gas
880 phase: technology for structural genomics and proteomics. *Chem Rev* **107**, 3544-67 (2007).
- 881 58. Maier, J.A. et al. ff14SB: Improving the Accuracy of Protein Side Chain and Backbone
882 Parameters from ff99SB. *J Chem Theory Comput* **11**, 3696-713 (2015).
- 883 59. Tsui, V. & Case, D.A. Theory and applications of the generalized born solvation model in
884 macromolecular simulations. *Biopolymers* **56**, 275-291 (2000).
- 885 60. Weiser, J., Shenkin, P.S. & Still, W.C. Approximate atomic surfaces from linear combinations
886 of pairwise overlaps (LCPO). *J Comput Chem* **20**, 217-230 (1999).
- 887 61. Irobalieva, R.N. et al. Structural diversity of supercoiled DNA. *Nat Commun* **6**, 8440 (2015).

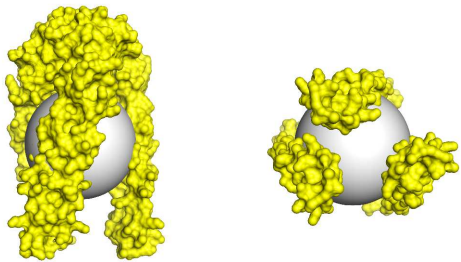
888

a**Skp****b****tOmpA**
8-stranded**c****PagP**
8-stranded**d****OmpT**
10-stranded**e****OmpF**
16-stranded**f****tBamA**
16-stranded*Extracellular**Periplasm**Extracellular**Periplasm*

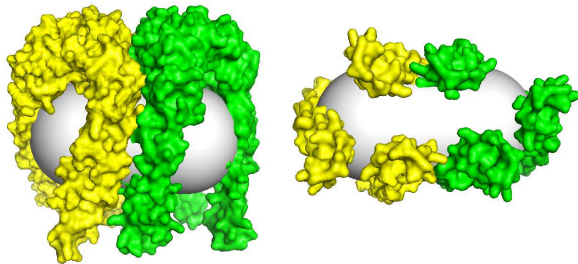
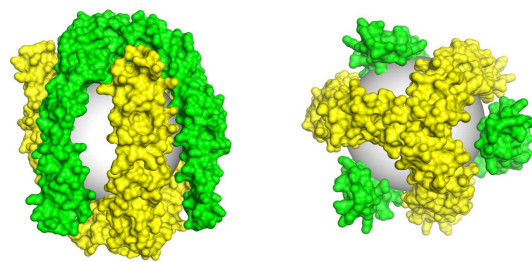
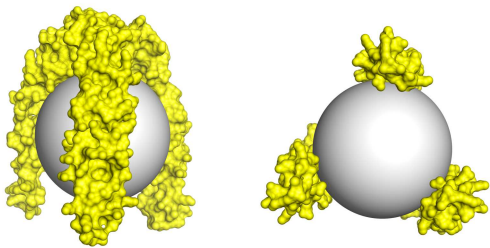
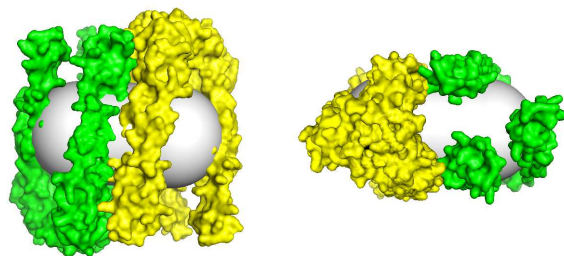
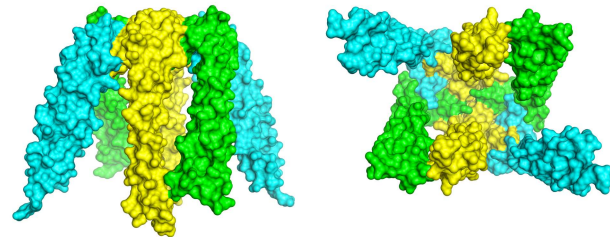






a

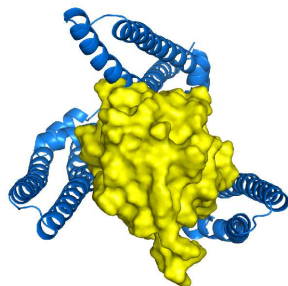
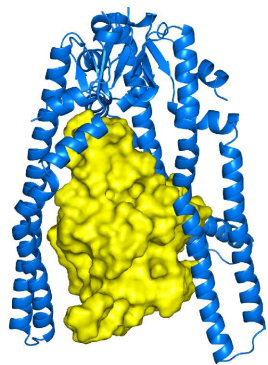
1:1 Skp:OMP

c2:1 Skp:OMP
side-by-side parallel**e**2:1 Skp:OMP
interlocked trimers**b**1:1 Skp:OMP
expanded cavity**d**2:1 Skp:OMP
side-by-side antiparallel**f**

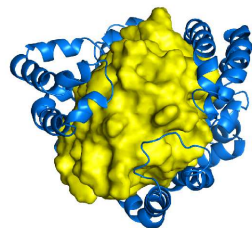
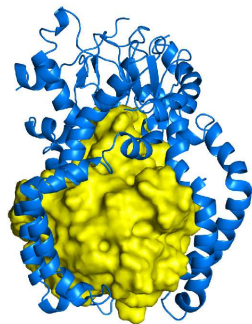
Prefoldin

a

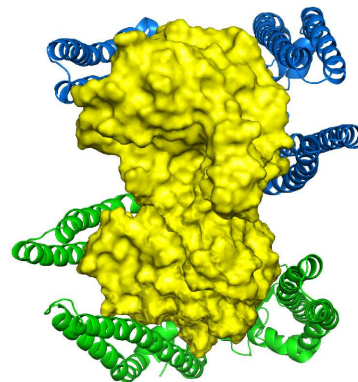
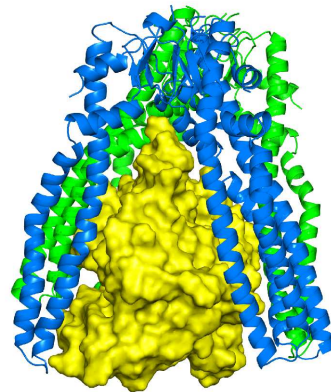
1:1 Skp:tOmpA
 $t = 0$

**b**

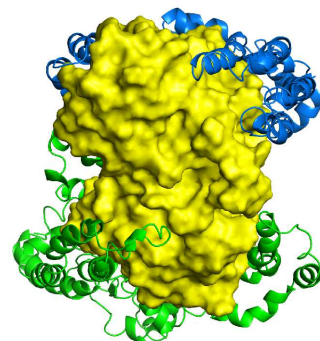
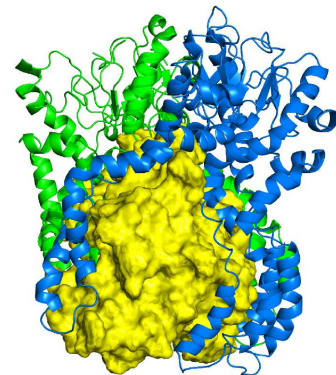
1:1 Skp:tOmpA
 $t = 10 \text{ ns (in vacuo)}$

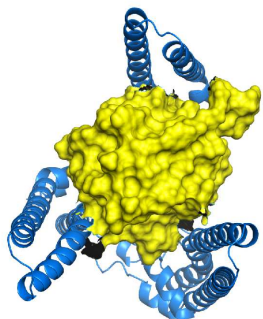
**c**

2:1 Skp:tBamA
 $t = 0$

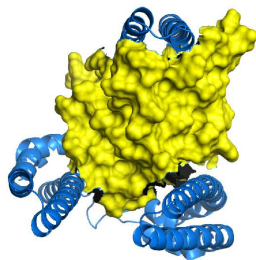
**d**

2:1 Skp:tBamA
 $t = 10 \text{ ns (in vacuo)}$

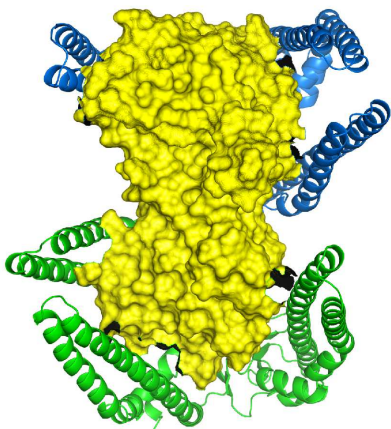


a

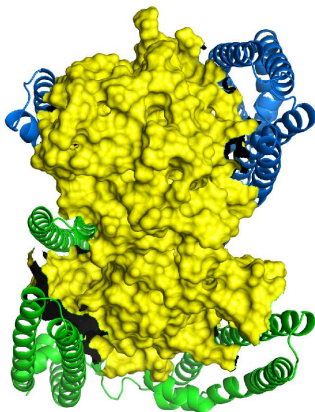
1:1 Skp:tOmpA
 $t = 0$



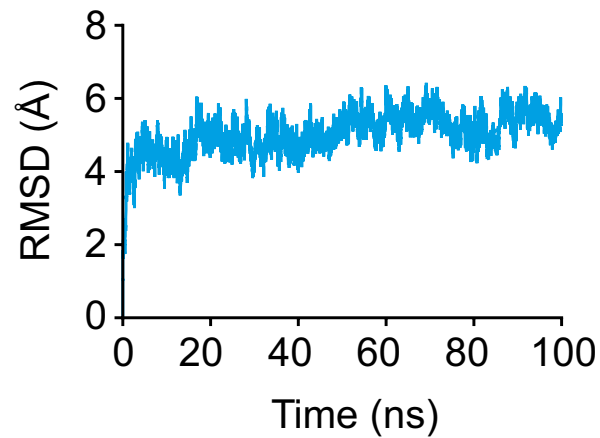
1:1 Skp:tOmpA
 $t = 100 \text{ ns (in solvent)}$

b

2:1 Skp:tBamA
 $t = 0$



2:1 Skp:tBamA
 $t = 100 \text{ ns (in solvent)}$

c**d**